DYNAMIC STRESS ANALYSIS IN THE ROOT REGION OF A TURBINE BLADE

by

JAY PRASHANT SHRIVASTAVA

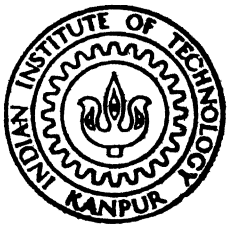

DEPARTMENT OF MECHANICAL ENGINEERING

INDIAN INSTITUTE OF TECHNOLOGY, KANPUR

SEPTEMBER, 1989

DYNAMIC STRESS ANALYSIS IN THE ROOT REGION OF A TURBINE BLADE

A Thesis Submitted
in Partial Fulfilment of the Requirements
for the Degree of
MASTER OF TECHNOLOGY

by
JAY PRASHANT SHRIVASTAVA

to the
DEPARTMENT OF MECHANICAL ENGINEERING
INDIAN INSTITUTE OF TECHNOLOGY, KANPUR
SEPTEMBER, 1989

CERTIFICATE

11/9/89.

This is to certify that the thesis entitled, 'Dynamic Stress Analysis in The Root Region of A Turbine Blade' by Jay Prashant Shrivastava is a bonafide record of work done by him under our guidance and supervision and has not been submitted elsewhere for the award of a degree.

(Dr. P. M. DIXIT)
Assistant Professor
Dept. of Mech. Engg.
Indian Institute of Technology
Kanpur - 208016

(Dr. N. S. VYAS)
Assistant Professor
Dept. of Mech. Engg.
Indian Institute of Technology
Kanpur - 208016

ACKNOWLEDGEMENTS

I express my gratitude to Dr. P. M. Dixit and Dr. N. S. Vyas for their inspiring guidance , invaluable suggestions , constructive criticism and being constant source of encouragement throughout this work.

I thank Dr. N. N. Kishore for allowing me to use the printer of ESA Lab.

I thank all my friends for helping me throughout my stay over here.

I greatly appreciate the excellent and neat tracings of Mr. B. K. Jain.

– J. P. Shrivastava.

CONTENTS

LIST OF TABLES

LIST OF FIGURES

NOMENCLATURE

A	Area of Cross-section
b	Distance from the Neutral Axis
C_v	Proportional Damping Coefficient
C_1, C_2, C_3	constants
E	Young's Modulus
F_c	Centripetal force
f_i	Shape function
F_y	Forcing function
h	Axial thickness
I	Moment of inertia
l	Blade length
n_s	Number of nozzles
p_i	Natural frequency in i^{th} mode
q	Time function
R_1	Outer radius of the disc
R_2	Inner radius of the disc
r, θ	polar coordinates
t	Time
T	Total Kinetic energy
T_I	Kinetic energy due to inertia effects
T_C	Kinetic energy due to centripetal effects
u, w	Displacements in X and Z directions
U	Strain energy
u_r	Radial displacement
V	Potential energy
W_d	Energy dissipated
W_p	Work done by external force
x, y, z	Cartesian coordinates
Y	Bending displacement in Y direction
Z_1	Blade length considered in root domain
Z	Distance along the blade length
$\bar{Z}$	Z / l
α	Angle made by tangential direction at the

	contact node with X-axis
$\varepsilon_r, \varepsilon_\theta$	Radial and Circumferential strain
ρ	Density
ω	Angular frequency
μ	Coefficient of friction
$\bar{\varepsilon}$	Clearance
Ω	Domain of the problem
Γ	System boundary
ν	Poisson's ratio
υ	Nozzle passing frequency
ζ	Damping ratio
ψ	Angle of pretwist
η	Generalised coordinates
σ_a, σ_m	Alternating and mean stress
σ_r, σ_θ	Radial and circumferential stress
[B]	Matrix containing derivatives of the shape functions
[C]	Damping matrix
[D]	Matrix containing material constants
[K]	Stiffness matrix
[M]	Mass matrix
[N]	Matrix Containing shape functions
[U]	Modal matrix
$\{B_f\}$	Body force vector
{f}	Traction Force Vector
{F}	Force vector
{Q}	Forcing vector
{U}	displacement vector
$\{\varepsilon\}$	Strain vector
$\{\sigma\}$	Stress vector

Subscript and superscript :

A	Body A
B	Body B
e	Elemental
i,j,k	Dummy indices
n,s	Normal and tangential direction
T	Transpose

ABSTRACT

To determine the dynamic stresses and displacements in the root region of a turbine blade, it is not enough to carry out the dynamic analysis of the blade alone. Because of the change in the geometry and interaction with the disc, this analysis is not valid in the root region. Instead, the region consisting of appropriate portions of the blade and the disc has to be analysed as a contact problem. The individual analysis of the blade and the disc provide the stress boundary conditions for the contact problem.

In this work a general computer program is developed to analyse first

(i) the blade as a cantilever beam and the disc as a body in axisymmetric plane stress and then

(ii) a thin layer of the root region as a plane stress problem by the finite element method.

The finite element segment of the program is tested by solving a simple problem with known results. This segment is also tested for convergence with respect to mesh size. The results are presented in the form of normal and tangential displacements and normal and shear stresses at the contact interface both for the mean as well as alternating stress boundary conditions. The variation of the contact displacements and stresses is obtained with respect to the following two parameters :

(a) rotor speed and

(b) domain geometry.

CHAPTER I

INTRODUCTION

1.1 Introduction :

It is widely recognized that fatigue failure of blades is a major cause of downtime in turbomachines. Such failures can be very costly in terms of lost production and replacement of parts. Dewey and Rieger [1] made a survey which revealed that high cycle fatigue alone is responsible for atleast 40 % failures in high pressure stages of steam turbines. Blade failures due to fatigue are predominantly vibration related and suppression of vibration must be a high priority item for reducing the number of industrial blade failures.

Blade vibrations are known to be caused by a number of different excitation mechanisms such as nozzle passing frequency excitation, partial admission operation, stall flutter, etc. Any of these sources may cause resonance with some natural frequency and give rise to large dynamic stresses. Blade fatigue usually initiates in a region of high stress at some structural or metallurgical discontinuity. If such conditions sustain for a sufficient number of load cycles, the local fatigue crack may continue to grow until failure occurs.

The earlier design practice has been to avoid fatigue by tuning the blade to operate away from the natural frequencies.

However in a typical turbomachine this may not always be possible for it may have three to four rotors, each having several stages and thus the turbine may altogether have a thousand blades with different characteristics. The dynamic stress analysis of the blade, then, becomes imperative. The blades in a turbomachine are connected to the disc by an attachment region called as blade root. The dynamic stress field in blades is known to be a function of a number of geometrical and operational parameters viz. cross-sectional areas, moments of inertia, operational speed, vibrational modes etc.

In steam turbines the disc being rigid relative to the blades, the blade vibration resembles that of a cantilever and though the dynamic stresses are dependent on the various geometric and operational parameters, it is often likely that the maximum stresses would occur at the blade root, especially in the fundamental vibratory mode which is most dangerous. Blade root is thus, a region vulnerable to failure. The complex shape of the root e.g. Tee, Fir-tree, Dove tail causes further stress concentration at the bends or sharp corners in the region. Moreover, the interfacial friction with the disc in the root region and the resulting wear aggravates the vulnerability of the root region.

The blade centrifugal load transmitted to the disc via interlocking hooks on either side of the root. The blade root also serves the purpose of providing damping, particularly at low centrifugal loads, to suppress the critical stresses, both during the machine starting/stopping as well as steady rotor operations.

All this necessitates stress analysis of the root region.

Such a stress analysis would further facilitate comparative studies of different types of roots.

1.2 Literature Survey :

1.2.1 Blade vibration :

Two distinct approaches towards the blade vibration problem have been (i) continuum modal approach and (ii) discrete modal approach. In the first approach the Lagrange's equation is formulated using the plate or beam theory and the solution of equation is obtained directly by approximate methods like Rayleigh-Ritz, Collocation, Ritz-Galerkin or by forming a set of first order differential equations by linear transformation and solving them by numerical integration, as in [2]. In the second approach, solution is obtained by any one of the following methods : Holzer-Myklestad Method, Finite Difference Method, Finite Element Method (special case of Rayleigh-Ritz or Galerkin), Transfer Matrix Method , Polynomial Frequency Equation Method etc. as in [3].

While free vibration analysis procedures are fairly well established for beam type of blades more work is necessary to establish the dynamic behavior of rotating pretwisted plate type of blades. A summary paper by Leissa et al [4] compares the existing methods for blades with small aspect ratio.

Blade damping is an important parameter in the fatigue design of blades since it is the damping that dictates the resonant stress levels. The main damping mechanisms are (i)

interfacial damping at the root, (ii) material damping and (iii) steam/gas dynamic damping. The superposition of these mechanisms determines the stress level achieved in resonant vibration and establishes the extent of susceptibility of the blade for fatigue failure. Possible contribution of these mechanisms are infinitely variable and no predictive theory exists presently to relate these damping mechanisms to specific blade damping properties.

Rao et al [5] devised an experimental method to obtain the overall damping coefficients of rotating blades in vibrational modes of various rotating speeds and vibrational amplitudes. It shows a decrease in damping coefficient with an increase in the speed of rotation, the existence of the threshold speed up to which frictional damping effect is most predominant and an increase in damping coefficients for higher modes of vibration, see Rao and Vyas [6].

Free vibration characteristics along with damping are used to determine the blade response due to a specific excitation force. Rieger and Nowak [7] used ANSYS program to determine the dynamic stresses. Matsura [8] and Hoyniak and Fleeter [9] have done work on blade resonant vibrations.

1.2.2 Contact Problems :

Determination of stresses and displacements in the root region of the blade is to be treated as a contact problem. For simple geometries, analytical methods for contact problems are discussed in Gladwell [10] and Muskhelishvili [11]. When the geometry of the contact region is complex , it becomes necessary

to use the finite element method. Chan and Tuba [12] proposed a finite element stiffness method for solving contact problems with friction. S. Ohte [13] proposed a method in which the contact interface is classified into adhering state and sliding state according to the reaction force acting on the contact surface and the friction coefficient. Francavilla and Zienkiewicz [14] solved the frictionless case of contact problems as a quasi-linear problem. N. Okamoto and M. Nakazawa [15] proposed a finite element incremental contact analysis with various frictionless conditions, considering the contact conditions as additional conditions independent of the stiffness equations. Huge and Sauxe [16] used FEM and mathematical programming technique to solve frictionless contact problems. Here appropriate linearization of the contact conditions is adopted and the problem is solved as a non iterative optimization problem. Sachdeva and Ramkrishnan extended the method of Francavilla and Zienkiewicz to take into account the force boundary conditions [17]and the frictional effects under proportionate loading [18]. Torstenfelt [19] proposed a general purpose finite element computer program to solve contact problem with friction. Rahman et al [2Ø] used finite element incremental procedure for contact analysis where the contact condition at a node is established when it numerically penetrates or touches a rigid body. Hence one body is considered rigid here. Chandrasekhara et al [21] solved the contact problem by imposing geometric constraints on the pseudo equilibrium configuration defined as a configuration at which the compatibility conditions are violated.

1.3 Objective and scope of present work :

The present work is an attempt to determine the dynamic stresses and displacements in the root region of a turbine blade. The study is restricted to the idealized case of a uniform cross-section long blade mounted on a uniform thickness disc rotating at a constant angular velocity. By carrying out the dynamic analysis of blade as a cantilever beam mounted on a rotating support, the stresses can be determined to a reasonable accuracy but only in the region sufficiently far away from the root. Because of the change in the geometry and interaction with the disc, this analysis is not valid in the root region. Therefore, the root region is analysed as a contact problem. The domain for this problem is chosen to include appropriate portions of the blade and the disc surrounding the actual contact area. Just like on any other boundary, on the boundary which separates the domain from the rest of the blade, either the displacements or the stresses have to be known. Here the stresses are used as the boundary condition . These stresses are obtained from the dynamic analysis of the blade as a cantilever beam mounted on a rotating support. For this, it is necessary that this boundary be sufficiently far away from the actual contact area, so that the individual blade analysis becomes valid there. The boundary which separates the domain from the rest of the disc is also chosen similarly and the stresses on this boundary are obtained from the analysis of the disc as a body in the state of axisymmetric plane stress.

The domain of the contact problem is a plate-like region

of variable thickness subjected to the stresses acting in the plane of the plate. However, this is not exactly a plane stress problem because of the following reason. The dynamic stresses in the blade consist of a mean and an alternating part and the alternating part varies across the thickness of blade. As stated earlier, these stresses become the boundary conditions for the analysis of the contact problem. Since the stresses on a part of the boundary are constant, the problem does not exactly fall into the category of the plane stress. However, every small layer of the domain can be considered as a plane stress problem. Since the alternating stresses are maximum at the extreme layers, one of these layers is chosen for the analysis. The chosen layer has tensile stresses on the boundary. In summary, a thin layer of appropriate portions of the blade and disc surrounding the actual contact surface is used as a domain for the analysis of the contact problem as a plane stress problem.

In the blade analysis, the beam theory is used to obtain the kinetic and potential energy terms in the Lagrange's equation of motion for free vibrations. The damping is assumed to be constant for all modes of vibration. The excitation (nozzle) forces are assumed to be harmonic and concentrated at the blade tip. The modal analysis is used to obtain the equations of forced vibrations which are solved using standard techniques. In the disc analysis, the equation of motion is expressed in terms of the radial displacements and solved analytically. Because of complex geometry, the contact problem is solved by finite element method. This method is a modification of the approach suggested by Sachdeva and Ramakrishnan [18]. They have used the flexibility

matrix in their analysis which is obtained by inverting the conventional stiffness matrix. However, in the present analysis, the stiffness matrix is retained as such. The matrix substructuring technique is used to condense the stiffness matrix for optimum storage and computational efficiency. Appropriate contact conditions involving friction are applied in an iterative scheme to the condensed stiffness matrix. Finally the contact stresses are obtained by averaging their magnitudes over the bodies in contact.

A general computer program is developed to determine
(i) natural frequencies, mode shapes, displacements and stress fields in the blade,
(ii) stress field in the disc, and
(iii) stress and displacement fields in the contact region.

The blade displacement and stress fields are obtained as functions of the rotational speed. The disc stresses are represented as functions of the radial coordinates for the various rotational speeds. Before applying the finite element segment of the program to the contact region, it was tested for a simple problem with known results. Further, the convergence of the method with respect to the mesh size was checked numerically. In the contact domain, the results are presented in the form of normal and tangential displacements and normal and shear stresses at the contact interface for various values of the rotor speeds. The results for mean and alternating boundary conditions are presented separately. In addition, the effects of varying the contact domain clearances on the interfacial displacements and stresses are studied. The variation of clearances is caused

either by changing the blade root dimensions or the disc groove dimensions.

This work has several limitations in the form of idealizations made and methodologies used.

1. The blade is idealized as a uniform thickness cantilever beam mounted on a rotating support. The actual blade is tapered, twisted with an asymmetric aerofoil cross-section and at times may be too short to be treated as a beam.

2. The disc is considered as a uniform thickness body in the state of axisymmetric plane stress. However, because of a finite number of blades, it is not exactly axisymmetric. There is also some change in the thickness.

3. The contact region is treated as a plane stress problem. But, because of the reasons mentioned above, it is not strictly a plane stress problem. It has not been ensured that a small shift in the boundaries with the blade or the disc has no appreciable change in the contact stresses and displacements. Further, the energy loss due to friction is not considered. Finally the iterative scheme used for the contact problem, although accounts for friction and slip, does not consider the incremental loading.

1.4 Plan of the Thesis :

The formulation of the blade, disc and contact problems and the solution procedure are described in chapter 2. The results and discussion are given in chapter 3, while the conclusions and the suggestions for future work in chapter 4.

CHAPTER II

THE PROBLEM

The problem of the dynamic stress analysis of the root region of a turbine blade is restricted here to the idealised case of a uniform cross-section cantilever beam mounted on a uniform thickness disc rotating at a desired constant angular velocity. (Fig. 2.1)

The disc can be analysed as an axisymmetric body subjected to a radial centripetal force due to its rotation. The rotation of the disc also induces a steady or mean stress on the blade. In addition the blade experiences alternating stresses due to its vibration on application of lateral external periodic forces from the nozzles. The state of stress obtained for such a system by analysis of its individual components i.e. the blade and the disc would however not hold good in the root region where the mutual interaction of the disc and blade and the resulting change in geometry have to be accounted for. The root region is hence to be treated as a contact problem. The contact domain should include appropriate portions of the disc and blade surrounding the actual contact area. Such a domain is demarcated by boundaries AB and CDEF in Fig. 2.1. The stresses obtained by the individual analysis of the blade and the disc are to be used as boundary conditions for the contact problem. It is necessary that the boundaries of the domain are sufficiently removed from the actual contact area for the individual blade and disc analysis to be valid at the boundaries.

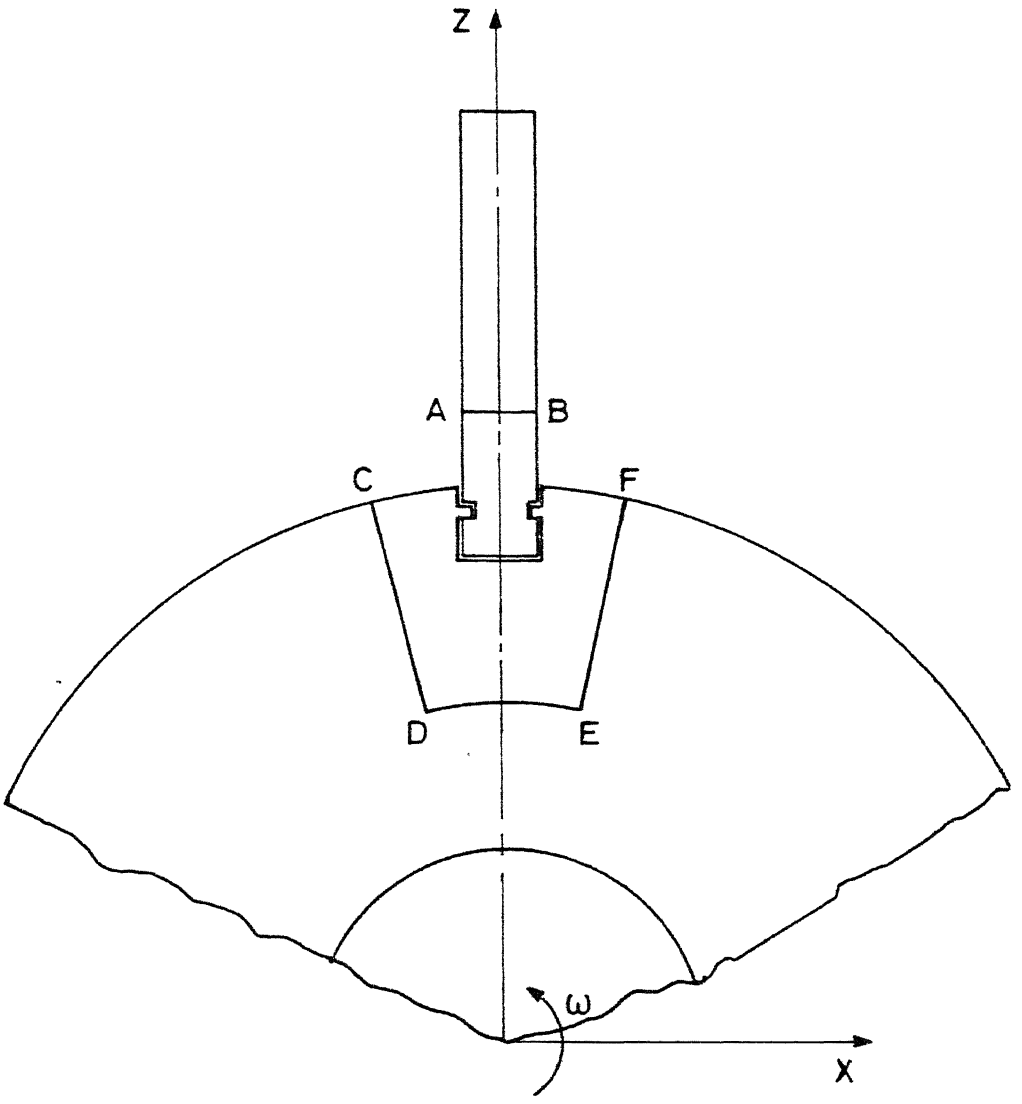

Fig. 2.1 Root domain for the contact problem.

2.1 The Blade :

The blade is treated as a uniform thickness cantilever beam mounted on a rotating disc Fig.(2.2a). The kinetic and potential energy terms for the blade are setup using beam theory and equation of Lagrange is employed to generate the eigenvalue problem. For ease of analysis damping is assumed to be constant for all modes of vibration and the nozzle forces are assumed to be harmonic and concentrated at the blade tip. Modal analysis is employed to obtain the equations of forced vibrations and the stress and displacement fields on the blade are obtained using standard techniques.

The potential energy of the vibrating beam is given by

$$V = \frac{1}{2}EI \int_{\emptyset}^{l} (y'')^2 \, dZ \qquad (2.1)$$

The kinetic energy T, can be seen to be constituted of two components - T_I, due to inertia effects and T_C, due to the centripetal effects. i.e.

$$T = T_I + T_C \qquad (2.2)$$

The component due to the inertia effects readily is

$$T_I = \frac{1}{2} \rho A \int_{\emptyset}^{l} (\dot{y})^2 \, dZ \qquad (2.3)$$

while the component due to the centripetal effects is the work done against the centripetal force i.e.

$$T_C = \int_{\emptyset}^{l} (dF_C) \, u \qquad (2.4)$$

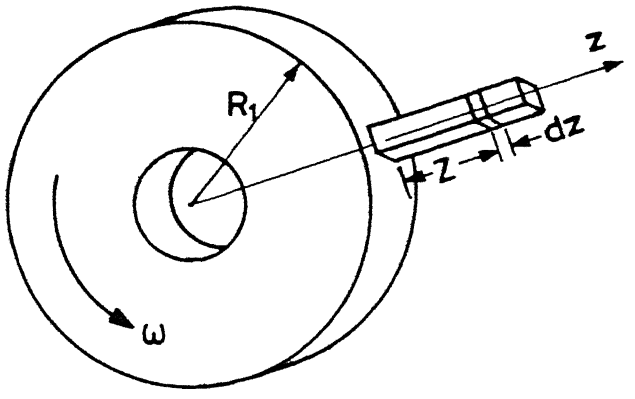

Fig.2.2(a) Blade mounted on a rotating disc.

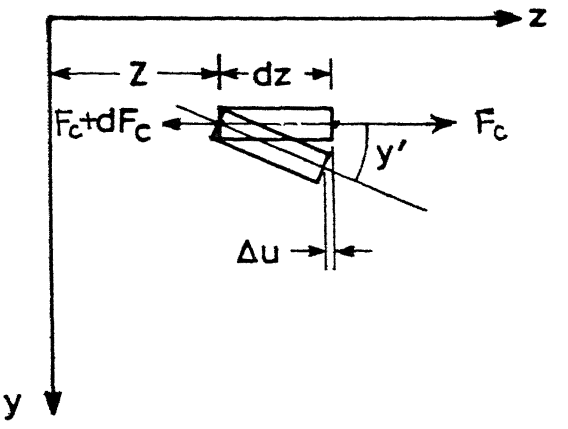

Fig.2.2(b) Bending of a blade element.

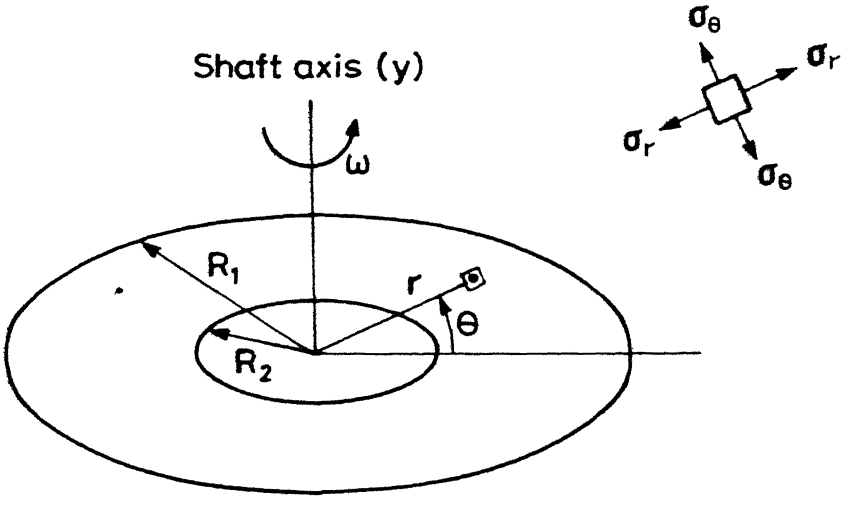

Fig.2.3 Rotatig disc .

where dF_C is the centripetal force on a small element of thickness dZ at a distance Z from the root(Fig 2.2b)

From Fig 2.2

$$\Delta u = dZ\ (1-\cos y')$$

$$\cong -\frac{dZ}{2}\ (y')^2$$

Thus

$$u = -\int_{\emptyset}^{Z} \frac{(y')^2}{2}\, dZ \qquad (2.5)$$

The centripetal force on the element is given by

$$dF_C = \rho\ \omega^2\ A\ (R_1 + Z)dZ \qquad (2.6)$$

Substitution of (2.5) and (2.6) in (2.4) and simplification gives

$$T_C = -\frac{1}{2}\ \rho\omega^2 A\int_{\emptyset}^{l}(y')^2\ [R_1(1 - Z) + \frac{1}{2}\ (l^2 - Z^2)]\ dZ \qquad (2.7)$$

Assuming a series form displacement field for the blade we have

$$y = \sum q_i(t)\ f_i(Z) \qquad (2.8)$$

where $q_i(t)$ is a time function and $f_i(Z)$ is the shape function given by

$$f_i(Z) = \frac{(i+2)(i+3)}{6}\ \bar{Z}^{i+1} - \frac{i(i+3)}{3}\ \bar{Z}^{i+2} + \frac{i(i+1)}{6}\ \bar{Z}^{i+3} \qquad (2.9)$$

with $\bar{Z} = \frac{Z}{l}$

The assumed shape function satisfies the boundary conditions of a cantilever.

From equations (2.1) to (2.3) and (2.7) to (2.9) we have

$$V = \frac{1}{2}\ EI \int_{\emptyset}^{l} \left[\sum_i q_i f_i'' \right]^2 dZ \qquad (2.1\emptyset)$$

and

$$T = \frac{1}{2}\rho A\int_{\emptyset}^{1}\left[\sum_{i}\dot{q}_i f_i\right]^2 dZ - \frac{1}{2}\rho A\omega^2\int_{\emptyset}^{1}\left[R_1(1-Z) + \frac{1}{2}(l^2 - Z^2)\right]\left[\sum_{i} q_i f_i'\right]^2 dZ \tag{2.11}$$

The equation of Lagrange is given by

$$\frac{d}{dt}\left[\frac{\partial T}{\partial \dot{q}}\right] - \frac{\partial T}{\partial q} + \frac{\partial V}{\partial q} = \emptyset \tag{2.12}$$

Substitution of (2.1Ø) and (2.11) in (2.12) yields the eigenvalue problem

$$[\ M\ ]\{\ \ddot{q}\ \} + [\ K\ ]\{\ q\ \} = \emptyset \tag{2.13}$$

where

$$M_{ij} = \rho\ A \int_{\emptyset}^{1} f_i f_j\ dZ \qquad \text{;and}$$

$$K_{ij} = \rho\ \omega^2 A \int_{\emptyset}^{1} [R_1(1-Z) + \frac{1}{2}\ (l^2 - Z^2)]\ f_i'\ f_j'\ dZ + EI\int_{\emptyset}^{1} f_i''\ \ f_j''\ \ dZ \tag{2.14}$$

The eigenvalue problem of equation (2.13) is solved to obtain the natural frequencies and mode shapes.

For ease of formulation damping is assumed to be viscous and proportional, such that the energy dissipated is

$$W_d = \frac{C_v T}{\rho} \tag{2.15}$$

where C_v is proportional damping coefficient.

The equation of motion for damped vibration can then be written as

$$[\ M\ ]\{\ \ddot{q}\ \} + [\ C\ ]\{\ \dot{q}\ \} + [\ K\ ]\{\ q\ \} = \emptyset \tag{2.16}$$

with $$[C] = \frac{C_v}{\rho} [M]$$

The excitation force is periodic with nozzle passing frequency υ (= $n_s\omega$). It is assumed to be harmonic in nature and concentrated at the free end of the blade such that

$$F_y(Z,t) = F_\emptyset \text{ Sin } \upsilon t \qquad \text{for } Z = 1$$
$$= \emptyset \qquad \text{for } Z \neq 1 \qquad (2.17)$$

The virtual work done by this external force is

$$\delta W_f = \int_\emptyset^1 (F_y \delta_y)\, dZ$$

$$= \{ Q_\emptyset \} \text{ Sin } \upsilon t$$

where $$\{ Q_\emptyset \} = \{F_\emptyset (f_i)_{Z=1}\} \qquad (2.18)$$

The equation for forced vibration then is

$$[M]\{ \ddot{q} \} + [C]\{ \dot{q} \} + [K]\{ q \} = \{ Q_\emptyset \} \text{Sin } \upsilon t \qquad (2.19)$$

The forced vibration problem can be solved using modal analysis.

If $$\{ q \} = [U]\{ \eta \} \qquad (2.2\emptyset)$$

where [U] = Modal matrix

then

$$[M][U]\{ \ddot{\eta} \} + [C][U]\{ \dot{\eta} \} + [K][U]\{ \eta \} = \{Q_\emptyset\} \text{Sin } \upsilon t \qquad (2.21)$$

Premultiplication by $[U]^T$ gives

$$[\bar{M}]\{ \ddot{\eta} \} + [\bar{C}]\{ \dot{\eta} \} + [\bar{K}]\{ \eta \} = \{ Q_{\emptyset N} \} \text{ Sin } \upsilon t \qquad (2.22)$$

where

$$[\bar{M}] = [U]^T [M][U]$$
$$[\bar{C}] = [U]^T [C][U]$$
$$[\bar{K}] = [U]^T [K][U]$$

$$\{ Q_{\emptyset N} \} = [U]^T \{ Q_{\emptyset} \} \qquad (2.23)$$

Hence the decoupled equation of motion can be written as

$$\bar{M}_j \ddot{\eta} + \bar{C}_j \dot{\eta} + \bar{K}_j \eta = Q_{\emptyset N_j} \text{ Sin } \upsilon t \qquad (2.24)$$

for which the solution is

$$\eta_j = \frac{(Q_{\emptyset N_j} / \bar{M}_j)}{\sqrt{(p_j^2 - \upsilon^2)^2 + 4 \zeta_j^2 p_j^2 \upsilon^2}} \text{ Sin } (\upsilon t - \psi_j) \qquad (2.25)$$

where

$$\zeta_j = \frac{\bar{C}_j}{2 \bar{M}_j p_j} \quad ; \text{ and}$$

$$\psi_j = \text{Tan}^{-1} \left[\frac{2 \zeta_j p_j \upsilon}{p_j^2 - \upsilon^2} \right]$$

The displacement field can be obtained by using equation (2.25) in conjunction with equations (2.2Ø) and (2.8)

The alternating stress field at any blade cross-section at any distance b from the neutral axis of the cross-section can be obtained using the formula

$$\sigma_a = E b y'' \qquad (2.26)$$

The mean stress field induced in the blade due to disc rotation can be evaluated as fallow .

The centripetal force on a small element of length dZ at a distance Z from the root of the blade is given by (Eq. 2.6)

$$dF_c = \rho \omega^2 A (R_1 + Z) dZ \qquad (2.6)$$

Therefore

$$F_c = \int_{Z_1}^{1} \rho \omega^2 A (R_1 + Z) dZ$$

$$= \rho\, \omega^2\, A \left[R_1 Z + \frac{Z^2}{2} \right]_{Z=Z_1}^{Z=1}$$

The mean stress experienced by the blade then is

$$\sigma_m = \frac{F_c}{A}$$

$$= \rho\, \omega^2 \left[R_1\, (1-Z_1) + \frac{(1^2-Z_1^2)}{2} \right] \qquad (2.27)$$

2.2 The Disc :

The disc is assumed to be of uniform thickness clamped at its centre on a shaft which is rotating at a constant angular velocity ω about the Y-axis (Fig. 2.3). The disc is in a state of axisymmetric as well as plane stress. There is only one nontrivial equation of motion. In terms of stress components, it is given by

$$\frac{d\,\sigma_r}{d\,r} + \frac{\sigma_r - \sigma_\theta}{r} + \rho\, \omega^2 r = \emptyset \qquad (2.28)$$

Since it is one equation in two unknowns, it cannot be solved in the present state. However, it can be solved by expressing it in terms of the radial displacements.

For the axisymmetric plane stress problem, the stress-strain relations are

$$\sigma_r = \frac{E}{1 - \nu^2} (\varepsilon_r + \nu\, \varepsilon_\theta)$$

$$\sigma_\theta = \frac{E}{1 - \nu^2} (\varepsilon_\theta + \nu\, \varepsilon_r) \qquad (2.29)$$

and the strain displacement relations are

$$\varepsilon_r = \frac{d\,u_r}{d\,r} \quad ; \quad \varepsilon_\theta = \frac{u_r}{r} \tag{2.30}$$

Substituting the relations (2.29) and (2.30) into (2.28) we get

$$\frac{E}{1-\nu^2}\,\frac{d}{d\,r}\left[\frac{1}{r}\,\frac{d}{d\,r}\,(r\,u)\right] + \rho\,\omega^2\,r = 0 \tag{2.31}$$

the solution of this equation is

$$u_r = -\,\frac{1-\nu^2}{E}\,\rho\,\omega^2\,\frac{r^3}{8} + C_1\,r + \frac{C_2}{r} \tag{2.32}$$

where C_1 and C_2 are constants of integration.

Substituting the expression (2.32) for the radial displacement into the equation (2.30) and (2.29) we get the following expression for stresses

$$\sigma_r = C_1\,\frac{E}{1-\nu} - \frac{C_2}{r^2}\,\frac{E}{1+\nu} - \frac{3+\nu}{8}\,\rho\,\omega^2\,r^2 \tag{2.33}$$

$$\sigma_\theta = C_1\,\frac{E}{1-\nu} + \frac{C_2}{r^2}\,\frac{E}{1+\nu} - \frac{1+3\nu}{8}\,\rho\,\omega^2\,r^2 \tag{2.34}$$

The constants C_1 and C_2 are to be determined from the boundary conditions. Since the shaft to which the disc is attached relatively more rigid than the disc, at the boundary $r=R_2$ the boundary condition becomes

$$u_r = 0 \quad \text{at} \quad r = R_2 \tag{2.35}$$

the boundary $r = R_1$ is stress free. Therefore

$$\sigma_r = 0 \quad \text{at} \quad r = R_1 \tag{2.36}$$

Using these conditions, we get

$$C_1 = \frac{1-\nu}{1+\nu}\,\frac{C_2}{R_1^2} + \frac{(3+\nu)(1-\nu)}{8\,E}\,\rho\,\omega^2\,R_1^2 \tag{2.37}$$

with

$$C_2 = -\frac{(1-\nu^2)\rho\,\omega^2\,R_1^2\,R_2^2}{8E}\left[\frac{(3+\nu)R_1^2 - (1+\nu)R_2^2}{(1+\nu)R_1^2 + (1-\nu)R_2^2}\right] \qquad (2.38)$$

Finally, after substituting the values of the constants, the expressions for stresses becomes

$$\sigma_r = (R_1{}^2 - r^2)\left[C_3 - \frac{E\,C_2}{(1+\nu)\,R_1{}^2\,r^2}\right] \qquad (2.39)$$

$$\sigma_\theta = \frac{C_3}{r^2}\left[\left[R_1{}^2 + \frac{E\,C_2}{(1+\nu)\,R_1^2\,C_3}\right]r^2 + \frac{E\,C_2}{(1+\nu)\,C_3} - \frac{1+3\nu}{3+\nu}\,r^4\right] \qquad (2.40)$$

where

$$C_3 = \frac{3+\nu}{8}\,\rho\,\omega^2 \qquad (2.41)$$

2.3 FEM Formulation :

2.3.1 Idealization of the Contact Problem as a Plane Stress Problem :

As stated earlier the stresses in the root region of the blade are to be determined by treating it as a contact problem. The domain of the problem is shown in Fig. 2.1. The domain is a plate like region of variable thickness subjected to the stresses acting in the plane of the plate. However, this is not exactly a plane stress problem because of the following reason. As mentioned before, the boundary conditions for the problem come from the analysis of the sections 2.1 and 2.2. Specifically, the boundary stresses on the boundary AB are obtained from the analysis of the blade described in section 2.1. There it is seen

that the alternating part of this stress varies across the thickness of the domain. Since the stresses on a part of the boundary are not constant across the thickness, the problem doesn't exactly fall into the category of plane stress. However, every small layer of the domain can be considered as a plane stress problem. Since the alternating stresses are maximum at the extreme layers, it is appropriate to use either of these layers for the analysis. Here the layer with tensile stresses on the boundary AB is considered. The analysis of the other extreme layer can be carried out in similar fashion but not have done in this work.

Henceforth it should be understood that the domain for the contact problem is a thin layer of the blade and the disc in the vicinity of the contact surface whose cross-section is shown in Fig 2.1. Moreover the stresses on the boundary AB are tensile. Because of the complexity of the geometry, the finite element method is used for the analysis.

2.3.2 FEM solution procedure :

In FEM formulation, the governing equations (partial differential equations) are converted into an equivalent set of integral equations. There are two common procedures available for converting the governing equations into equivalent integral equations. These are (i) the variational procedure and (ii) the Galerkin procedure (or the method of weighted residues). The solution domain is divided into several small elements of chosen shape and the unknown field variables are expressed in terms of assumed approximating functions (or interpolation functions)

within each element. The approximating functions are defined within each element in terms of the field variables at specified points called as *nodes*. The nodal values of the field variables and the interpolation functions for the element completely define the behavior of the field variables within the element. For the finite element formulation of the problem, the nodal values of the field variables become the new unknown. The integral equations of the problem are evaluated within each element using the interpolation function for the element. All such elemental integrals are assembled to obtain the final matrix equation. The unknown nodal variables are calculated by solving the assembled matrix equation for the whole solution domain.

2.3.3 FEM Formulation for plane stress/strain :

Consider a body Ω of uniform thickness h bounded by two parallel planes Y=-h/2 and Y=h/2 and a closed boundary Γ (Fig. 2.4). The part of the boundary on which external stresses act is denoted by q . The body is in a state of plane stress.

In X-Z plane, the strain displacement relations are

$$\varepsilon_x = \frac{\partial u}{\partial x} \quad ; \quad \varepsilon_z = \frac{\partial w}{\partial z} \quad ; \quad \gamma_{xz} = \frac{\partial u}{\partial z} + \frac{\partial w}{\partial x}$$

In matrix form

$$\{ \varepsilon \} = [L] \{ u \} \qquad (2.42)$$

Where $\{ \varepsilon \} = \{ \varepsilon_x \quad \varepsilon_z \quad \gamma_{xz} \}^T$

$\{ u \} = \{ u \quad w \}^T$

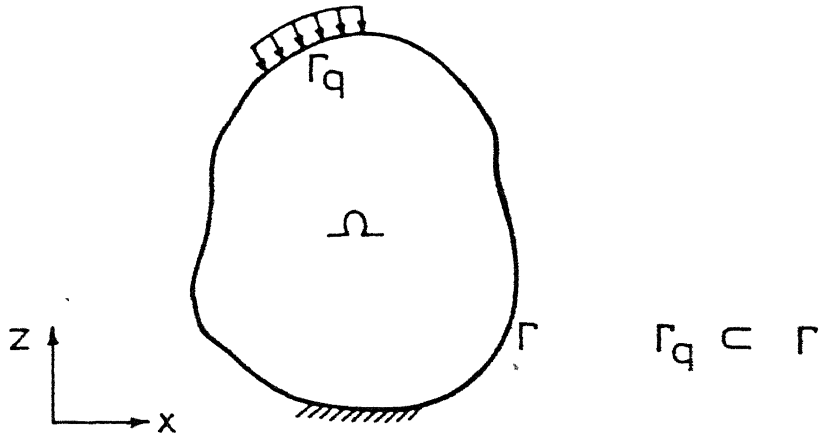

Fig. 2.4 Body in plane stress

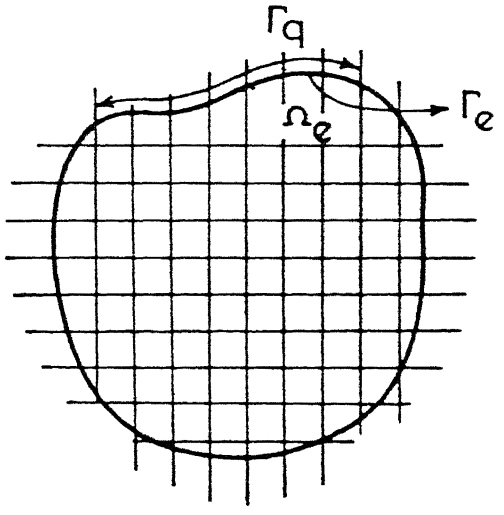

Fig. 2.5 Discretisation of the domain.

$$[\ L\ ] = \begin{bmatrix} \frac{\partial}{\partial x} & \emptyset \\ \emptyset & \frac{\partial}{\partial z} \\ \frac{\partial}{\partial z} & \frac{\partial}{\partial x} \end{bmatrix} \tag{2.43}$$

Then stress strain relationship for a homogeneous, isotropic, linearly elastic material under plane stress conditions is given by

$$\{\ \sigma\ \} = [\ D\ ]\ \{\ \varepsilon\ \} \tag{2.44}$$

Where $\{\ \sigma\ \} = \{\ \sigma_x \quad \sigma_z \quad \tau_{xz}\ \}^T$

and $$[\ D\ ] = \frac{E}{1-\nu^2} \begin{bmatrix} 1 & \nu & \emptyset \\ \nu & 1 & \emptyset \\ \emptyset & \emptyset & \frac{1-\nu}{2} \end{bmatrix} \tag{2.45}$$

The strain energy is

$$U = \int_{\Omega} \frac{1}{2}\ \{\ \varepsilon\ \}^T\ \{\ \sigma\ \}\ h\ dA \tag{2.46}$$

If

$$\left\{\ f\ \right\} = \begin{Bmatrix} f_x \\ f_z \end{Bmatrix} \quad \text{and} \quad \left\{\ B_f\ \right\} = \begin{Bmatrix} B_x \\ B_z \end{Bmatrix} \tag{2.47}$$

represent the applied traction on Γ_q and the body force (per unit volume) respectively, then the work done by the external forces is given as

$$W_p = \int_{\Omega} \{\ u\ \}^T\ \{\ B_f\ \}\ h\ dA + \int_{\Gamma_q} \{\ u\ \}^T\ \{\ f\ \}\ h\ dl \tag{2.48}$$

The expression for Potential Energy of the system is given as

$$\Pi_p = U - W_p \tag{2.49}$$

Using Eqs. (2.44), (2.46), and (2.48)

$$\Pi_p = \frac{1}{2}\int_{\Omega}\{\ \varepsilon\ \}^T[\ D\ ]\{\ \varepsilon\ \}hdA - \int_{\Omega}\{\ u\ \}^T\{\ B_f\ \}hdA - \int_{\Gamma_q}\{\ u\ \}^T\{\ f\ \}hdl \tag{2.50}$$

If the domain be divided into N_e number of elements (Fig.2.5), over a typical element e let

$$\{\ u\ \} = \begin{bmatrix} N_1 & \emptyset & \ldots & N_n & \emptyset \\ \emptyset & N_1 & \ldots & \emptyset & N_n \end{bmatrix} \begin{Bmatrix} u_1^e \\ w_1^e \\ \vdots \\ u_n^e \\ w_n^e \end{Bmatrix}$$

$$= [\ N\ ]\ \{\ u\ \}_{nodal} \tag{2.51}$$

be the approximation for the displacement vector, where n is the number of nodes per element u_1^e, w_1^e, ...u_n^e, w_n^e are the displacements at the nodes and N_1 . . N_n are the shape functions in the form of polynomials of the coordinates x and z. Then from equation (2.42), we get

$$\{\ \varepsilon\ \} = [\ B\ ]\ \{\ u\ \}_{nodal} \tag{2.52}$$

Where the matrix [B] contains the derivatives of the shape functions. Substituting Equations (2.51) and (2.52) in to the expression (2.50) for the potential energy, we get

$$\Pi_p = \sum_{e=1}^{Ne} \frac{1}{2}\, h \int_{\Omega_e} \{\ u\ \}^T_{nodal}\ [\ B\ ]^T\ [\ D\ ]\ [\ B\ ]\ \{\ u\ \}_{nodal}\ dA$$

$$- \sum_{e=1}^{N_b} h\int_{\Omega_e}\{\ u\ \}^T_{nodal}[\ N\ ]^T\{\ B_f\ \}dA - \sum_{e=1}^{N_b} h\int_{\Gamma_e}\{\ u\ \}^T_{nodal}\ [\ N\ ]^T\{\ f\ \}_{dl} \tag{2.53}$$

Here Γ_e is the boundary of an element which is common with Γ_q and N_b is the number of such elements. (Fig. 2.5).

Setting the first variation of Π_p to zero, we get

$$[K] \{ u \} = \{ \bar{F} \} \tag{2.54}$$

Where
$$[K] = \sum_{e=1}^{N_e} [K]^e \tag{2.55}$$

$$[K]^e = \int_{\Omega_e} [B]^T [D] [B] h \, d A_e \tag{2.56}$$

$$\{ F \} = \sum_{e=1}^{N_e} \{ F \}^e \tag{2.57}$$

$$\{ \bar{F} \}^e = \int_{\Omega_e} [N]^T \{ B_f \} h \, dA + \int_{\Gamma_e} [N]^T \{ f \} h \, dl \tag{2.58}$$

and $\{ U \}$ is the vector of nodal displacements for the entire domain.

In the equation (2.55) and (2.57), it is understood that the sum is performed after expanding $[K]^e$ and $\{ F \}^e$ to the full size.

The formulation of plane strain problem would be similar except that in this case the elasticity matrix $[D]$ would be

$$[D] = \frac{E(1-\nu)}{(1+\nu)(1-2\nu)} \begin{bmatrix} 1 & \frac{\nu}{(1-\nu)} & 0 \\ \frac{\nu}{(1-\nu)} & 1 & 0 \\ 0 & 0 & \frac{(1-2\nu)}{2(1-\nu)} \end{bmatrix} \tag{2.59}$$

2.3.4 Formulation of the Contact Problem :

Two bodies A and B which are in the state of plane stress/strain are in contact with each other as shown in Fig 2.6. The finite element equations for these bodies are

$$\left[K_A \right] \left\{ U_A \right\} = \left\{ F_A \right\} \qquad (2.60a)$$

$$\left[K_B \right] \left\{ U_B \right\} = \left\{ F_B \right\} \qquad (2.60b)$$

where $\left[K_A \right]$, $\left[K_B \right]$, $\left\{ U_A \right\}$, $\left\{ U_B \right\}$, $\left\{ F_A \right\}$, $\left\{ F_B \right\}$ are the stiffness matrices, displacement vectors and force vectors of bodies A and B respectively. The force vector includes the contact forces also.

The equations (2.60) cannot be solved as at the contact nodes, neither displacements nor forces are known. To overcome this difficulty, contact conditions are used.

The matrix equation for A and B can be combined into a single equation as

$$\begin{bmatrix} \left[K_A \right] & \emptyset \\ \emptyset & \left[K_B \right] \end{bmatrix} \begin{Bmatrix} \{U_A\} \\ \{U_B\} \end{Bmatrix} = \begin{Bmatrix} \{F_A\} \\ \{F_B\} \end{Bmatrix}$$

or $$[K]\{ U \} = \{ F \} \qquad (2.61)$$

2.3.4.1 Contact Conditions :

There are two sets of contact conditions, one on the

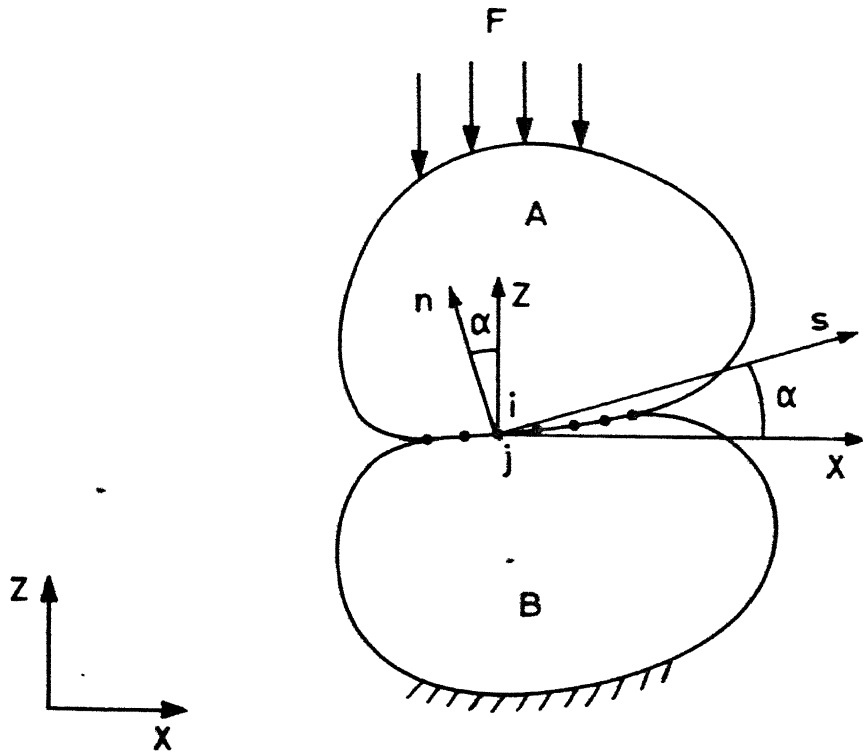

Fig. 2.6 Two bodies A and B in contact.

unknown contact forces and the other on the displacements. Let the i^{th} node of body A be in contact with the j^{th} node of body B. (Fig. 2.6) Let n and s denote respectively the normal and the tangential directions at the contact node. Then the conditions on forces, as given by Newton's third law, are

$$\left\{ F_A \right\}_{in} = - \left\{ F_B \right\}_{jn} \tag{2.62}$$

$$\left\{ F_A \right\}_{is} = - \left\{ F_B \right\}_{js} \tag{2.63}$$

The compatibility of displacement components gives the second set of condition

$$- \left\{ U_A \right\}_{in} + \left\{ U_B \right\}_{jn} = \bar{\varepsilon} \tag{2.64}$$

$$\left\{ U_A \right\}_{is} = \left\{ U_B \right\}_{js} \tag{2.65}$$

where $\bar{\varepsilon}$ denotes the clearance

The compatibility condition for the tangential direction is valid only when there is no slip between the contact nodes. The slip depends on the magnitude of the normal force at the node and the coefficient of friction between the bodies in contact. In the case of slip, the condition (Eq. 2.65) on tangential displacement should be replaced by the following relation

$$\left| \left\{ F_B \right\}_{js} \right| = \mu \left| \left\{ F_B \right\}_{jn} \right| \tag{2.66}$$

This condition can be applied to the body A also.

The contact conditions (2.62)-(2.66) are in terms of the components with respect to normal and tangential directions, while the finite elements equation (2.61) are with respect to x-z coordinate system. Therefore, first, these conditions must be expressed in terms of the x-z components. From the Fig.2.6, we get the following relations between the n-s components and x-z components.

$$(F_A)_{in} = -(F_A)_{ix} \text{ Sin } \alpha + (F_A)_{iz} \text{ Cos } \alpha \qquad (2.67)$$

$$(F_A)_{is} = (F_A)_{ix} \text{ Cos } \alpha + (F_A)_{iz} \text{ Sin } \alpha \qquad (2.68)$$

Here α is the angle which s-directions makes with x-axis. Similarly, the normal and tangential components of other forces and displacements can be expressed in terms of the x-z components. Substituting the Eq. (2.67)-(2.68) and similar relation for $(F_B)_{jn}$, $(F_B)_{js}$, $(U_A)_{in}$, $(U_A)_{is}$, $(U_B)_{jn}$ and $(U_B)_{js}$ into the Eq.(2.62)-(2.66), we get the following conditions

$$-(F_A)_{ix} \text{ Sin } \alpha + (F_A)_{iz} \text{ Cos } \alpha - (F_B)_{jx} \text{ Sin } \alpha + (F_B)_{jz} \text{ Cos } \alpha = \emptyset \qquad (2.69)$$

$$(F_A)_{ix} \text{ Cos } \alpha + (F_A)_{iz} \text{ Sin } \alpha + (F_B)_{jx} \text{ Cos } \alpha + (F_B)_{jz} \text{ Sin } \alpha = \emptyset \qquad (2.70)$$

$$(U_A)_{ix} \text{ Sin } \alpha - (U_A)_{iz} \text{ Cos } \alpha - (U_B)_{jx} \text{ Sin } \alpha + (U_B)_{jz} \text{ Cos } \alpha = \bar{\varepsilon} \qquad (2.71)$$

$$(U_A)_{ix} \text{ Cos } \alpha + (U_A)_{iz} \text{ Sin } \alpha - (U_B)_{jx} \text{ Cos } \alpha - (U_B)_{jz} \text{ Sin } \alpha = \emptyset \qquad (2.72)$$

$$(ss \text{ Cos } \alpha + \mu\, sn \text{ Sin } \alpha)(F_B)_{jx} + (ss \text{ Sin } \alpha - \mu\, sn \text{ Cos } \alpha)(F_B)_{jz} = \emptyset \qquad (2.73)$$

where ss is sign of $(F_B)_{js}$ and sn is sign of $(F_B)_{jn}$

Note that in case of no slip the condition(2.72) applies while the condition (2.73) is to be used when there is slip.

2.3.4.2 Application of contact conditions :

It can be seen that corresponding to every contact pair (i,j), there are four equations in the set (2.61). Two equations - (2i-1)th Eq. for x-direction and (2i)th Eq. for z-direction, for the body A and the remaining two (2j-1)th Eq. and (2j)th, for the body B. At stated earlier, neither the displacement associated with these nodes nor the forces(i.e. the right hand side of these equations) are known. Therefore, these equations can not be solved as such. However for every contact pair, there are four contact conditions. Our strategy is to replace these equations with unknown right hand sides by the contact conditions which have the known right hand side. The matrix operations required for this process are described below.

First we replace the (2i-1)th Eq. of body A by the Eq.(2.69). Since $(F_A)_{ix}$ and $(F_A)_{iz}$ are equal to the left hand sides of (2i-1)th and (2i)th Eq. of the body A and $(F_B)_{jx}$and $(F_B)_{jz}$are equal to the left hand side of (2j-1)th and (2j)th Eq. of body B, the condition states that

(-sinα) (2i-1)th Eq. of body A

+(cosα) (2i)th Eq. of body A

+(-sinα) (2j-1)th Eq. of body B

+(cosα) (2j)th Eq. of body B =Ø

Thus after replacement, the (2i-1)th row of the $[K_A]$ becomes equal to

$(-\sin\alpha)$(2i-1)th row of $[K_A]$

$+(\cos\alpha)$(2i) th row of $[K_A]$

$+(-\sin\alpha)$(2j -1) th row of $[K_B]$

$+(\cos\alpha)$(2j) th row of $[K_B]$

The (2i-1)th row of $[F_A]$, of course, becomes zero.

Next, the (2i)th Eq. of body A is replaced by the Eq. (2.7Ø). The matrix operations for this replacement are similar. Now, the (2i) th row of $[K_A]$ is replaced by the linear combination of (2i-1)th and (2i)th rows of $[K_A]$ and (2j-1)th and (2j) th rows of $[K_B]$, the coefficients of a linear combination given by the Eq. (2.7Ø). The (2i)th row of $[F_A]$, of course, becomes zero. Note that the Eq. (2.7Ø) involves the original (2i-1)th row of $[K_A]$ and not the modified one. Thus (2i-1)th row of $[K_A]$ has to be stored before applying the first contact condition.

The third condition is applied in the end. The reasons for this change of order will be explained later. So now, consider the fourth contact condition. We use this to replace (2j-1)th Eq. of body B. In case of no slip the condition is given by the Eq. (2.72). Since this Eq. is in terms of displacement components, we don't have to do any row operation like the first two conditions while using it for replacement. Instead,we simply have to replace the (2j-1)th row of $[K_B]$ by zeros except in the columns (2i-1), (2i), (2j-1) and (2j). In these columns, the new coefficients will be respectively $\cos\alpha$, $\sin\alpha$, $(-\cos\alpha)$ and $(-\sin\alpha)$. The (2j-1)th row of $[F_B]$, of course,. becomes zero. IN case of slip, the condition is given by the Eq. (2.73). This condition is similar to the first two conditions except that it involves only two Eq. : (2j-1)th and.(2j) th equations of body B. So here,

(2j-1)th row of $[K_B]$ is replaced by the linear combinations of (2j-1)th and (2j) th rows of $[K_B]$, the coefficients of the linear combination given by Eq. (2.73). The (2j-1)th row of $[F_B]$ is, of course, made zero. Finally, the (2j) th Eq. of body B is replaced by the third contact condition (Eq. 2.71). Since it is in terms of the displacement components, we simply have to replace the (2j)th row of $[K_B]$ by zeros. except in the columns (2i-1), (2i), (2j-1)and (2j) where the new coefficients will be $\sin\alpha$, $(-\cos\alpha)$, $(-\sin\alpha)$ and $\cos\alpha$. The (2j)th row of $[K_B]$ is made equal to $\bar{\varepsilon}$ (the clearance).

If we apply the third Eq. before the fourth, then the (2j)th Eq. of body B gets modified. In case of slip, the original (2j)th Eq. is needed to apply the fourth condition. So either we store the (2j)th row of $[K_B]$ and then apply the third and fourth condition in that order or we reverse the order and don't store the (2j)th row of $[K_B]$. The later alternative is more convenient and followed here.

2.3.4.3 Sub-structuring :

Since the number of contact nodes is initially unknown, an iterative procedure needs to be applied to the Eq. . (2.61). Further imposition of contact conditions renders the stiffness matrix unsymmetric. An iterative scheme involving large unsymmetric matrices requires a large storage and a considerable amount of computing time. To reduce both storage and computational time, the stiffness matrix is stored in skyline form and then decomposed to a much smaller size using substructuring.

First step in substructuring is to rearrange the rows and columns of the global stiffness matrix as shown below

$$\begin{bmatrix} K_{I,I} & K_{I.II} & K_{I,III} \\ K_{II,I} & K_{II,II} & K_{II,III} \\ K_{III,I} & K_{III,II} & K_{III,III} \end{bmatrix} \begin{Bmatrix} U_I \\ U_{II} \\ U_{III} \end{Bmatrix} = \begin{Bmatrix} F_I \\ F_{II} \\ F_{III} \end{Bmatrix} \quad (2.74)$$

Here the suffix I denotes the degree of freedom associated with contact nodes and the nodes at which non zero forces are specified, II denotes the degree of freedom associated with the free surface and internal nodes, while III denotes the degree of freedom associated with the nodes at which displacements are specified. If the prescribed displacements are zero then $U_{III} = \emptyset$

Further the nodal force at the free surface and internal nodes are zero i.e. $F_{II} = \emptyset$. Thus the Eq. (2.74) reduces to

$$K_{I,I}\, U_I + K_{I,II}\, U_{II} = F_I \quad (2.75)$$

$$K_{II,I}\, U_I + K_{II,II}\, U_{II} = \emptyset \quad (2.76)$$

Eliminating U_{II} from the above equations we get

$$\overline{K_{I,I}}\; U_I = F_I \quad (2.77)$$

where $$\overline{K_{I,I}} = (K_{I,I} - K_{I,II}\, K^{-1}_{II,II}\, K_{II,I}) \quad (2.78)$$

To obtain the matrix $\overline{K_{I,I}}$, $K_{I,I}$ is first extracted in full form from the global stiffness matrix in skyline form. Next $K_{II,II}$ is obtained in skyline form from the global stiffness

matrix. Then the matrix $K_{II,II}^{-1}K_{II,I}$ is obtained columnwise. If $\{ C \}_i$ is its i^{th} column, then it is obtained by solving the system

$$\left[K_{II,II} \right] \left\{ C \right\}_i = \left\{ K_{II,I} \right\}_{i^{th}Column} \qquad (2.79)$$

Thus the inverse of $K_{II,II}$ is not explicitly found. Next the elements of the matrix $K_{I,II}\ K_{II,II}^{-1}\ K_{II,I}$ are obtained by multiplying the rows of $K_{I,II}$ with the appropriate column of $K_{II,II}^{-1}\ K_{II,I}$. In this step as well as in the earlier step, we need the matrices $K_{I,II}$ and $K_{II,I}$ (these are transpose of each other). But these matrices are not determined explicitly. Instead their rows and columns are generated as and when required. Finally $\overline{K_{I,I}}$ is obtained using the Eq. (2.78).

Substructuring thus leads to a smaller set of equations (2.77). This set is solved after applying the contact conditions. Displacements U_{II} are obtained by back substituting U_I in the equation

$$U_{II} = - K_{II,II}^{-1}\ K_{II,I}\ U_I \qquad (2.80)$$

Once all the displacements are known F_{III} can be readily found using the third set of equation (2.74).

2.3.4.4 Contact Conditions Application Procedure :

The set of equations (2.77) are solved iteratively by applying the contact conditions in the following way

1. A set of nodal points is assumed to be in contact (it should include all possible contact points) and equations (2.77) are solved after applying the contact conditions where the fourth

condition is the no slip condition (eq. . 2.72).

2. The normal nodal forces cannot be tensile. Hence all those nodes where normal nodal forces come out to be tensile are deleted from the possible contact zone in the next iteration.

3. The ratio of the tangential nodal force to the normal nodal force is calculated at all the nodes in contact. If this ratio is greater than the coefficient of friction between the two surfaces at any node, it implies that this node is slipping in the tangential direction relative to the corresponding contact node. When a node slips in the next iteration, the contact condition (2.72) is replaced by (2.73). The other nodes are still governed by the condition (2.72).

The steps 2 and 3 are repeated until all the normal forces in the contact zone come out to be compressive and the ratio of the tangential force to the normal force for all the nodes in contact is either equal or less than the coefficient of friction. Once the iterations are over the stresses are computed.

2.3.4.5 Evaluation of Stresses :

To evaluate the stress at a point, first the vector $\{u\}_{nodal}$ for the element, to which the point belongs, is obtained from the solution vector { U } (the nodal displacement for the entire domain). Stresses are calculated by using equation (2.44) and (2.52) i.e.

$$\{ \sigma \} = [D] \{ B \} \{ u \}_{nodal} \qquad (2.81)$$

However, we need stresses in the contact region which is

nothing but a common boundary between the bodies A and B. Our approximating function for the displacements is such that the stresses do not become continuous across the interelement boundaries. Therefore we adopt the following procedure.

First we choose a set of points in the contact region such that the point belongs to only a single element of bodies A and B. Then the stress components σ_x, σ_z, τ_{xz} at these points are calculated first by assuming that they belongs to the body A and then to B. Next the components T_x and T_y are calculated by the relation

$$\begin{Bmatrix} T_x \\ T_z \end{Bmatrix} = \begin{bmatrix} \sigma_x & \tau_{xz} \\ \tau_{xz} & \sigma_z \end{bmatrix} \begin{Bmatrix} n_x \\ n_z \end{Bmatrix} \tag{2.82}$$

Here the unit normal vectors for bodies A and B will be in the opposite direction. Finally, the normal and tangential components of the stress vector { T } are calculated and their magnitudes are averaged over the bodies A and B.

CHAPTER III

RESULTS AND DISCUSSION

A general computer program is developed on the basis of the analysis presented in chapter 2. The program takes as inputs

(i) blade, disc and contact geometry

(ii) blade and disc material properties

(iii) rotational speed

(iv) damping and nozzle excitation data.

The output consists of

(i) natural frequencies and mode shapes of the blade

(ii) stress and displacement fields of the blade

(iii) stress field of the disc

(iv) stress and displacement fields in the contact domain.

The geometry and material properties of the blade disc model undertaken for this study is given in Fig. 3.1.

The blade displacement and stress fields are obtained as functions of rotational speed. The disc stresses are represented as functions of radial coordinate for various rotational speeds. The above stresses at appropriate stations form the boundary conditions for the contact domain problem. In the contact domain results are presented in the form of normal and tangential displacements and normal and shear stresses at contact interface. At the interface, points farthest from the central line experience maximum normal stresses, which for the present model are most critical. As stated in chapter 2 these results are obtained for

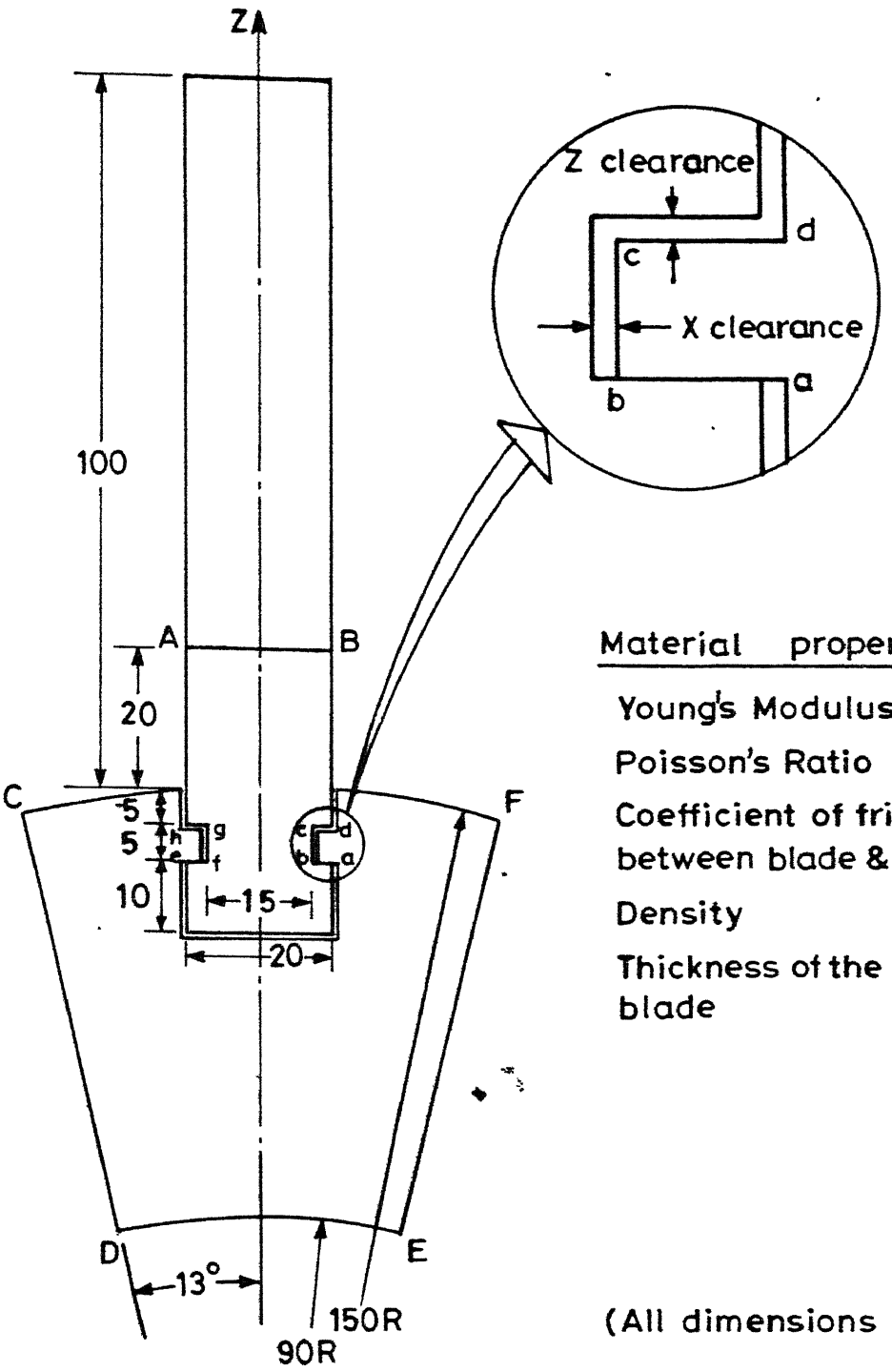

AB and CDEF boundaries define the root domain.

Material properties

Young's Modulus $E = 2 \times 10^5$ N/mm^2

Poisson's Ratio $\nu = 0.25$

Coefficient of friction between blade & disc $\mu = 0.2$

Density $\rho = 8 \times 10^{-6}$ kg/mm^3

Thickness of the blade $w = 3$ mm

(All dimensions are in mm)

Fig. 3.1 The Tee joint between the blade and the disc.

the outermost layer by treating the problem as one of plane stress. Similar exercise can be carried out for the inner layers of the blade-disc assembly. In addition the effect of varying the contact domain clearances on the interfacial displacements and stresses are studied. The variation of clearances is caused either by changing the blade root dimensions or the disc groove dimensions.

3.1 Stresses in the Blade :

In the program segment for the blade a five term series shape function (refer Eq. 2.8) is used which gives converged results for free as well as forced vibration response. Fig. 3.2 depicts the first four natural frequencies of the blade. The effect of rotor speed on natural frequencies is also shown. As expected the centripetal effect due to rotation causes a stiffening of the blade resulting in an increase in natural frequency. Fig. 3.3 is the Campbell diagram for the blade. The excitation is assumed to be a pure harmonic of the Nozzle Passing Frequency, NPF ($\nu=n_s\omega$) and the number of nozzles n_s is taken as 24. The intersection of the NPF line with the natural frequency curves gives the resonant rotor speeds which in this case are (6Ø2 RPM, 3285 RPM, 11Ø7Ø RPM, 23ØØØ RPM). As can be seen from Fig. 3.4, which plots the blade root stresses versus rotor speed, the intersection of the fundamental vibratory mode with the exciting NPF gives the most critical resonance at 6Ø2 RPM. The peaks for the resonances with higher vibratory modes become successively weaker. Fig. 3.5 shows that at 6Ø2 RPM the maximum dynamic stress

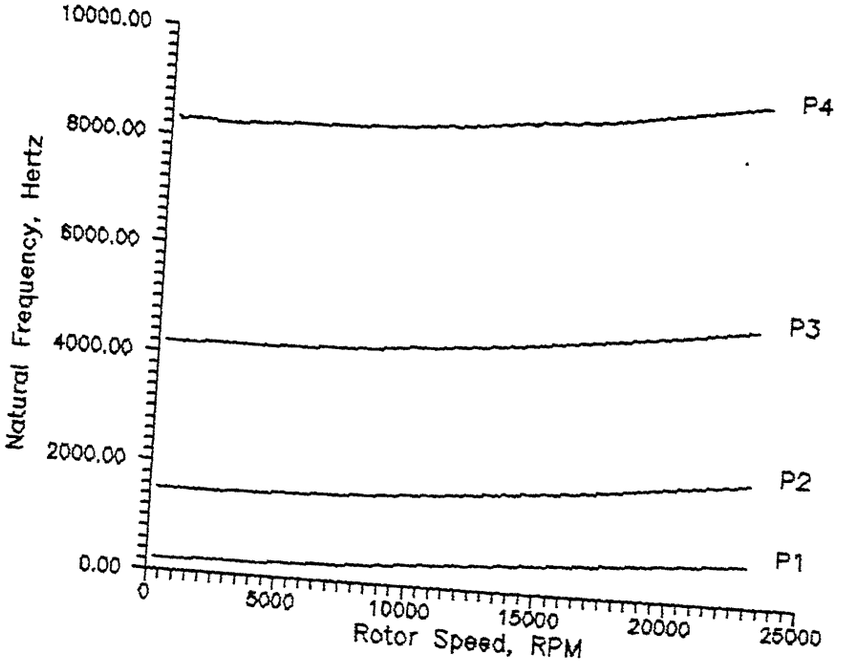

Fig.3.2 Variation of Natural Frequencies with Rotor Speed

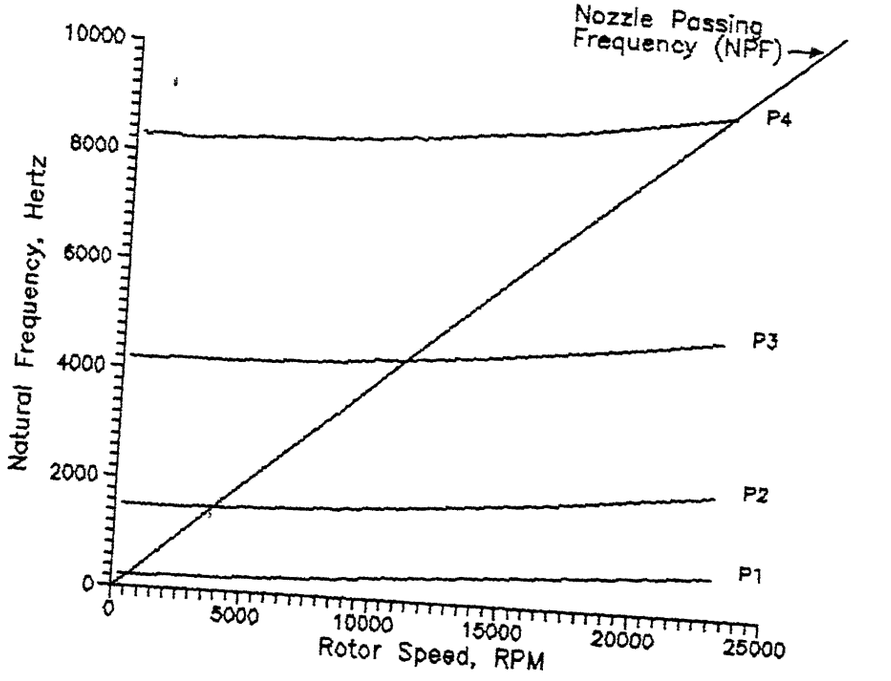

Number of nozzel (n_s) = 24
NPF (ν) = n_s w

Fig 3.3 Campbell – Diagram

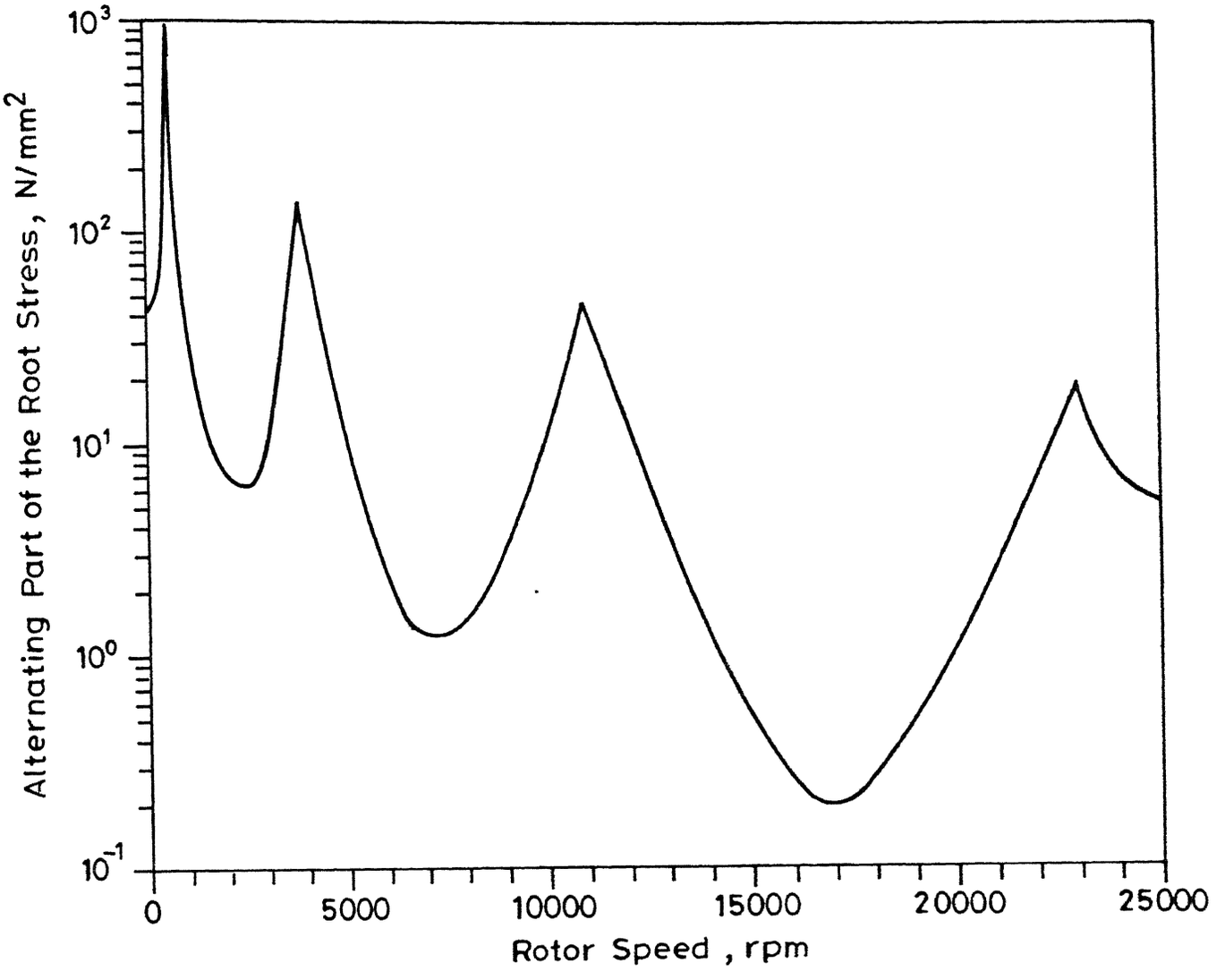

Fig. 3.4 Alternating part of the root stress vs. rotor speed.

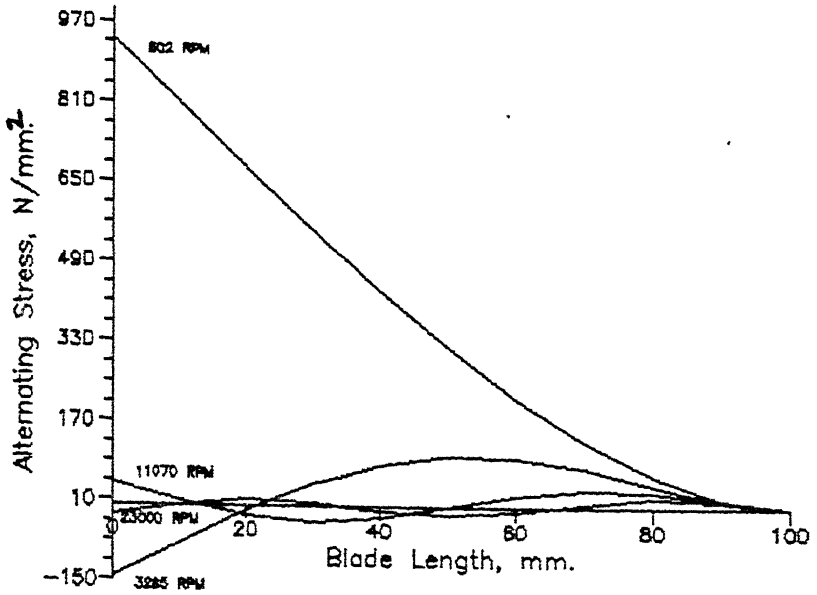

Fig.3.5 Variation of Alternating Stress along the Blade Length at Rotor Speeds corresponding to Natural Frequencies.

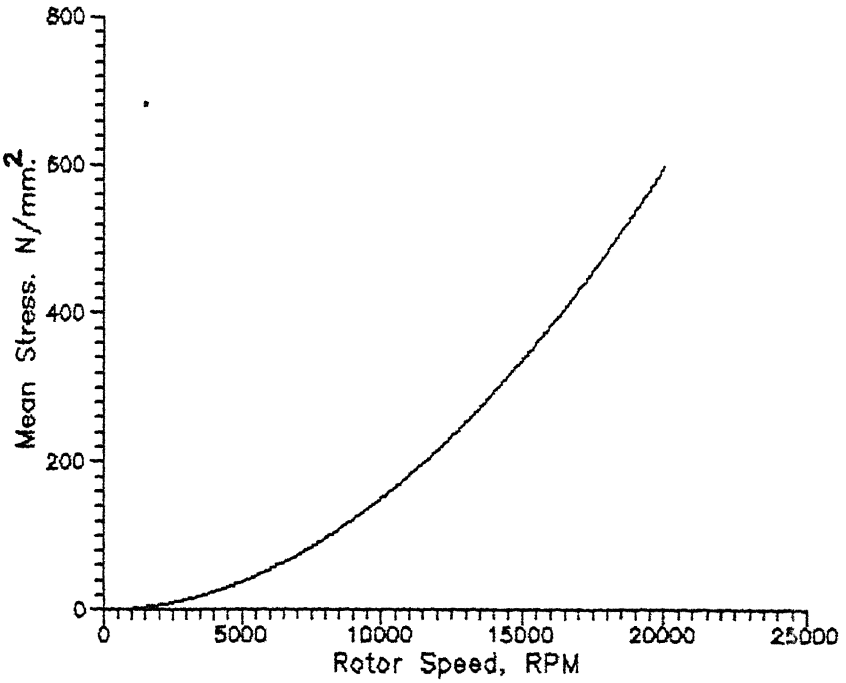

Fig.3.6 Variation of Mean Stress in the Root Region with Rotor Speed

in the blade occur at the root while at 3285 RPM the maximum dynamic stress does not occur at the root but at a point somewhat midway between the root and tip. This is so, for the resonance at 6Ø2 RPM is caused due to the interaction between the fundamental vibratory mode and the NPF while the resonance at 3285 RPM is caused due to the interaction of the second blade mode and the NPF. In fact the stress distributions along the blade length for various resonant speeds are a consequences of the shape acquired by the blade while vibrating in various cantilever modes.

Fig. 3.6 gives the mean stress experienced by the blade due to the rotational effect alone. The centripetal effect being more pronounced at higher speeds the mean stresses on the blade increase with an increase in rotational speed.

3.2 Stresses in the Disc :

The disc is in a state of axisymmetric plane stress. The radial and circumferential stresses as functions of radial coordinate are shown in Fig. 3.7 and 3.8 for a typical rotor speed of 6Ø2 RPM.

The blade and disc stresses thus obtained for a desired rotor speed at the boundaries AB and CDEF shown in Fig. 3.1 are input boundary conditions to the program segment for the root domain analysis.

3.3 FEM Program for the Contact Problem :

The program segment for the root domain is based on the

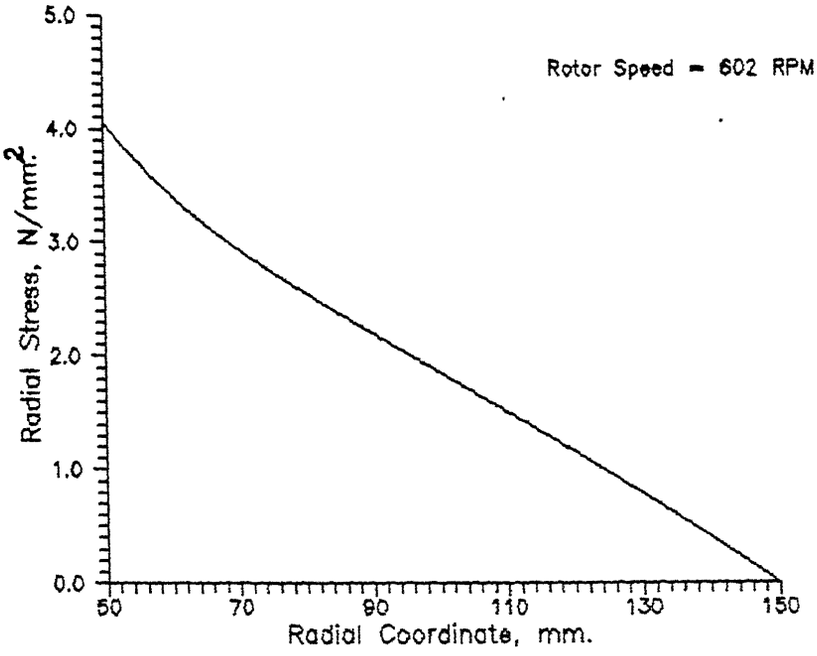

Fig.3.7 Variation of Radial Stress along the Radial Coordinate of the Disc.

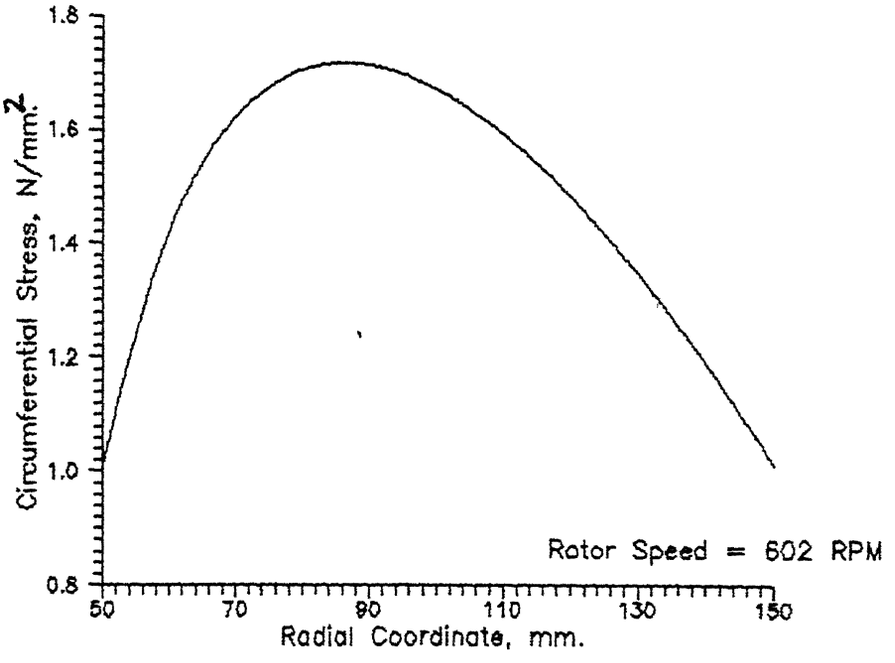

Fig 3.8 Variation of circumferential stress along the Radial Coordinate of the Disc.

finite element formulation described in chapter 2 to solve plane stress (or plane strain) contact problem with friction. The program uses four noded isoparametric elements and gives the displacement and forces at each node as well as normal and shear stress variation along the contact length.

3.3.1 Test Problem for the FEM Program :

Before application of the program to the blade root domain it was tested for a simple plane strain problem with known results. Two prismatic bodies of rectangular cross-section in contact and with a point load at their midspan were considered (Fig. 3.9). The finite element mesh for body A consists of 12 elements and 21 nodes while that of body B consists of 30 elements and 44 nodes. To begin with 7 nodes are assumed to be in contact. Four iterations are needed to converge to the correct solution. The converged solution shows that only 5 nodes are in contact. The displacements and stresses at the contact surface are in good agreement with those of Ramesh [25]. The plane stress version of the problem is solved by Sachdeva and Ramkrishnan [18] and the results for the plane stress version with present program match quite well with their results. The deformed shape of the two bodies in contact (on an enlarged scale) and the normal stress variation along the semi contact length are shown in Figs. 3.9 and 3.10.

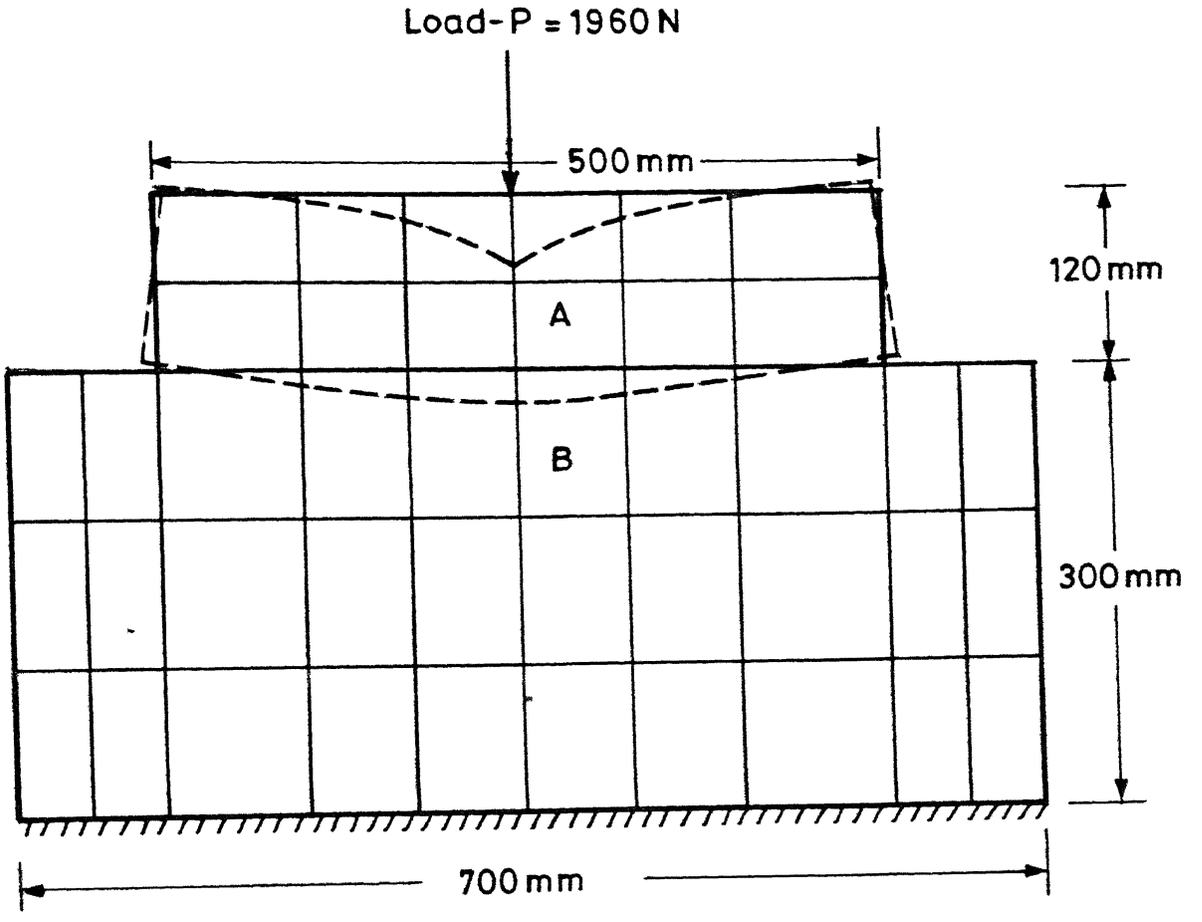

Material properties

Young's Modulus E = $0.931 \times 10^5 N/mm^2$

Poisson's Ratio = 0.25

Coefficint of friction $\mu = 0.20$

Deformation Scale

0 40 80 120 160 μm

Fig. 3.9 Finite element mesh and deformed shape for the test problem.

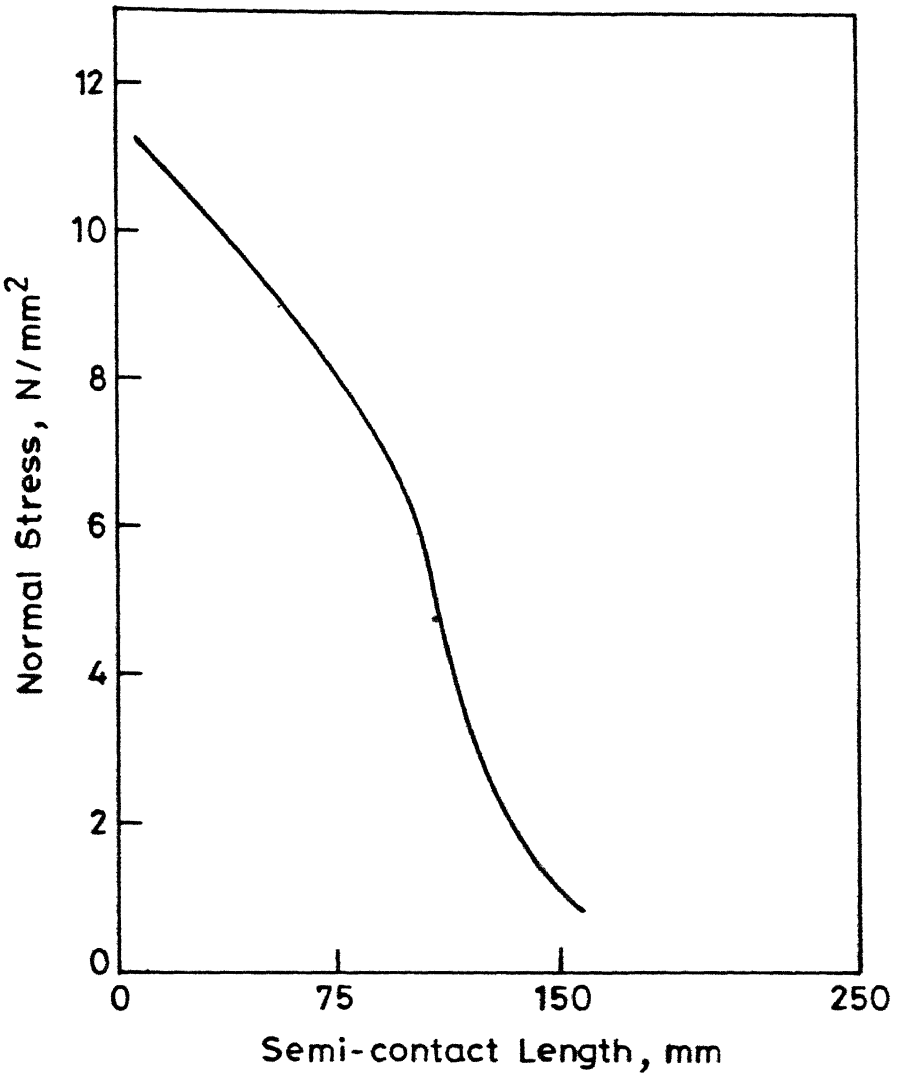

Fig. 3.10 Variation of normal stress along the semi-contact length for the test problem.

3.3.2 Convergence of the FEM Program :

Since the contact problem was a non-linear problem it is necessary to check the convergence of FEM Program results numerically with respect to mesh size. The convergence study was made for a rotor speed of 2000 RPM. The program was executed for the discretisations listed in Table 3.1

The variation of the normal and tangential displacements and stresses for all three discretisations are shown in Figs. 3.11. From the curves a very good and fast trend towards convergence can be seen. The numerical values of these quantities at selected points along the contact length are shown in Table 3.2.

The third finite element mesh shown in Fig 3.12 is chosen for carrying out further root domain analysis.

3.3.3 Results for the Contact Displacements and Stresses :

3.3.3.1 Mean Contact Displacements and Stresses :

The results for stresses and displacements for the contact interface of the blade disc assembly are given in Figs. 3.13 and 3.14. The results are presented for the semi contact length marked *ba* and *fe* in the Fig. 3.1. The lengths are measured from the Z-axis shown in Fig 3.1. Figures 3.13 depict the normal displacement, tangential displacement, normal stress and shear stress variation along the semi contact length for various speeds of rotation, when the mean stresses from the blade are given as

Table .3.1

Finite element discretisation for convergence study

Discretisation	Blade part		Disc part	
	Number of elements	Number of nodes	Number of elements	Number of nodes
I	26	42	4Ø	63
II	34	54	48	75
III	54	83	7Ø	1Ø6

Table : 3.2

Displacement values for different finite element discretisation

Distance from the centre line i.e.z-axis, mm.	Normal displacement $x1Ø^{-4}$mm.			Tangential displacement $x1Ø^{-4}$mm.		
	I^{st} Mesh	II^{nd} Mesh	III^{rd} Mesh	I^{st} Mesh	II^{nd} Mesh	III^{st} Mesh
7.75	2Ø.89	21.Ø43	21.1Ø6	2.Ø521	2.Ø476	2.Ø471
9.ØØ	17.161	17.2Ø9	17.225	3.8852	3.888Ø	3.8933
1Ø.Ø	13.3Ø3	13.256	13.239	4.9543	4.9779	4.99Ø1

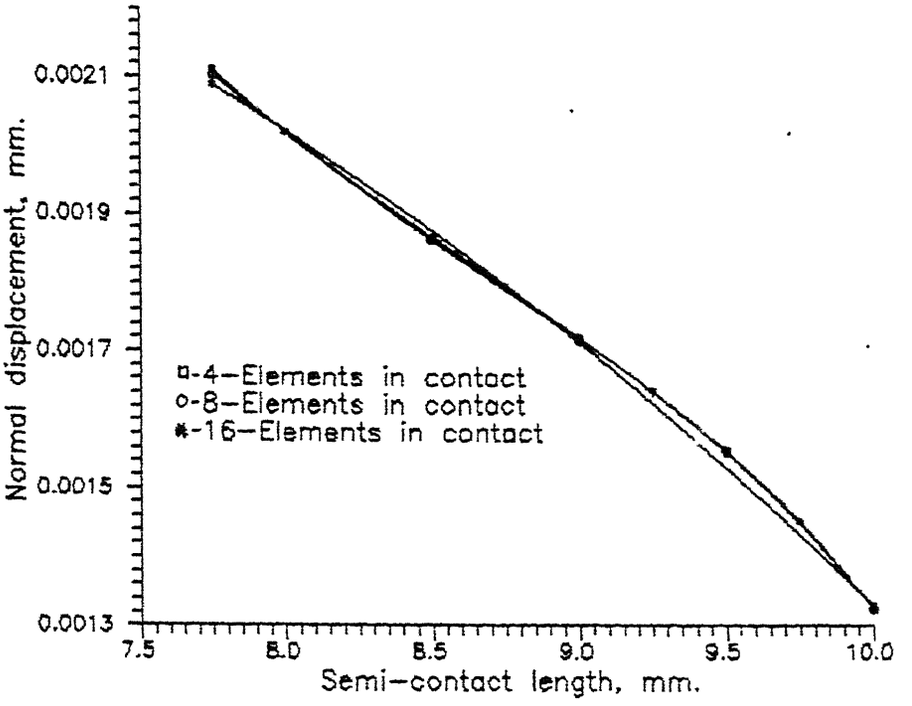

Fig.3.11(a) Variation of Normal Displacement along the Semi Contact Length for three Discretisations. (Convergence Study)

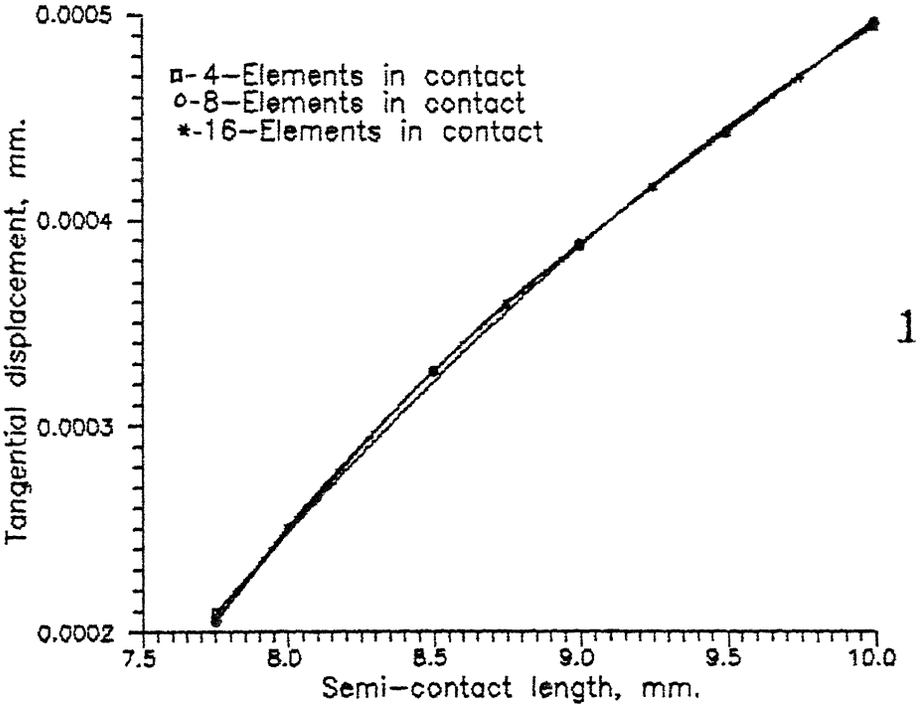

Fig.3.11(b) Variation of Tangential Displacement along the Semi Contact Length for three Discretisations. (Convergence Study)

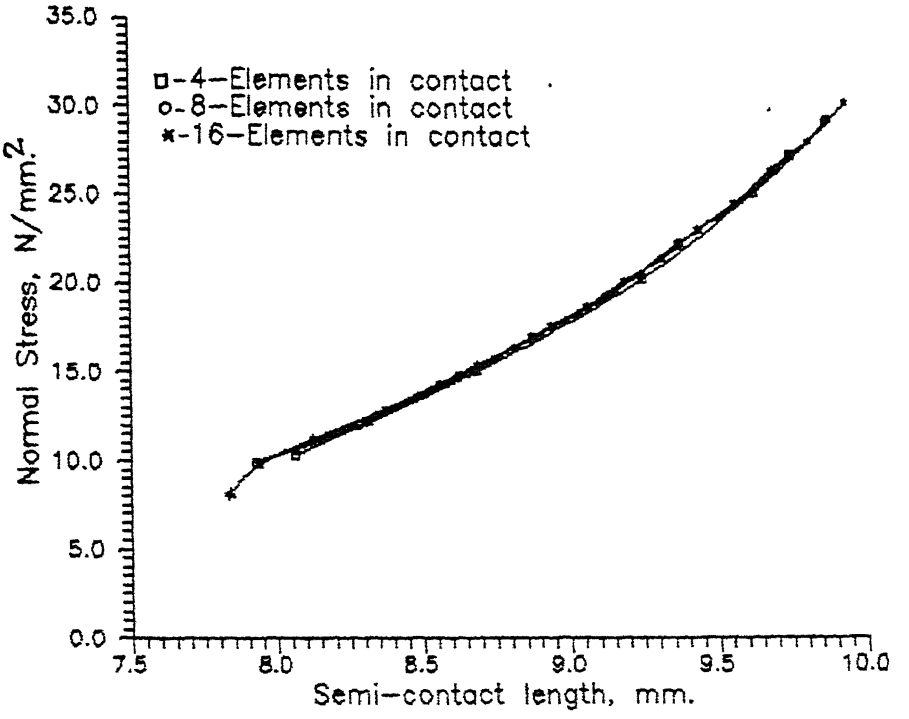

Fig.3.11(c) Variation of Normal Stress along the Semi Contact Length for three Discretisations. (Convergence Study)

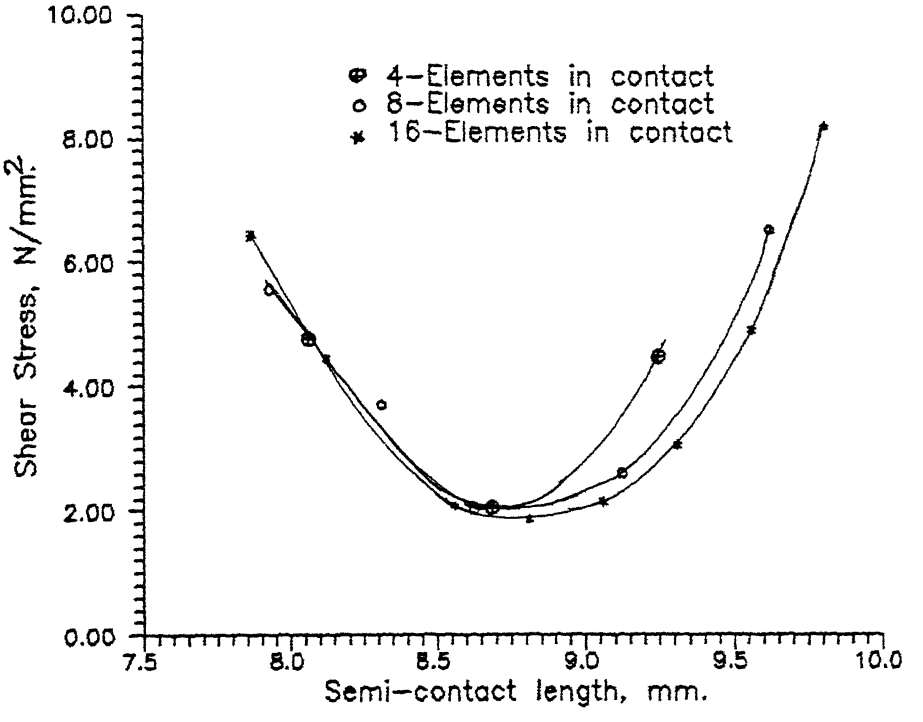

Fig.3.11(d) Variation of Shear Stress along the Semi Contact Length for three Discretisations. (Convergence Study)

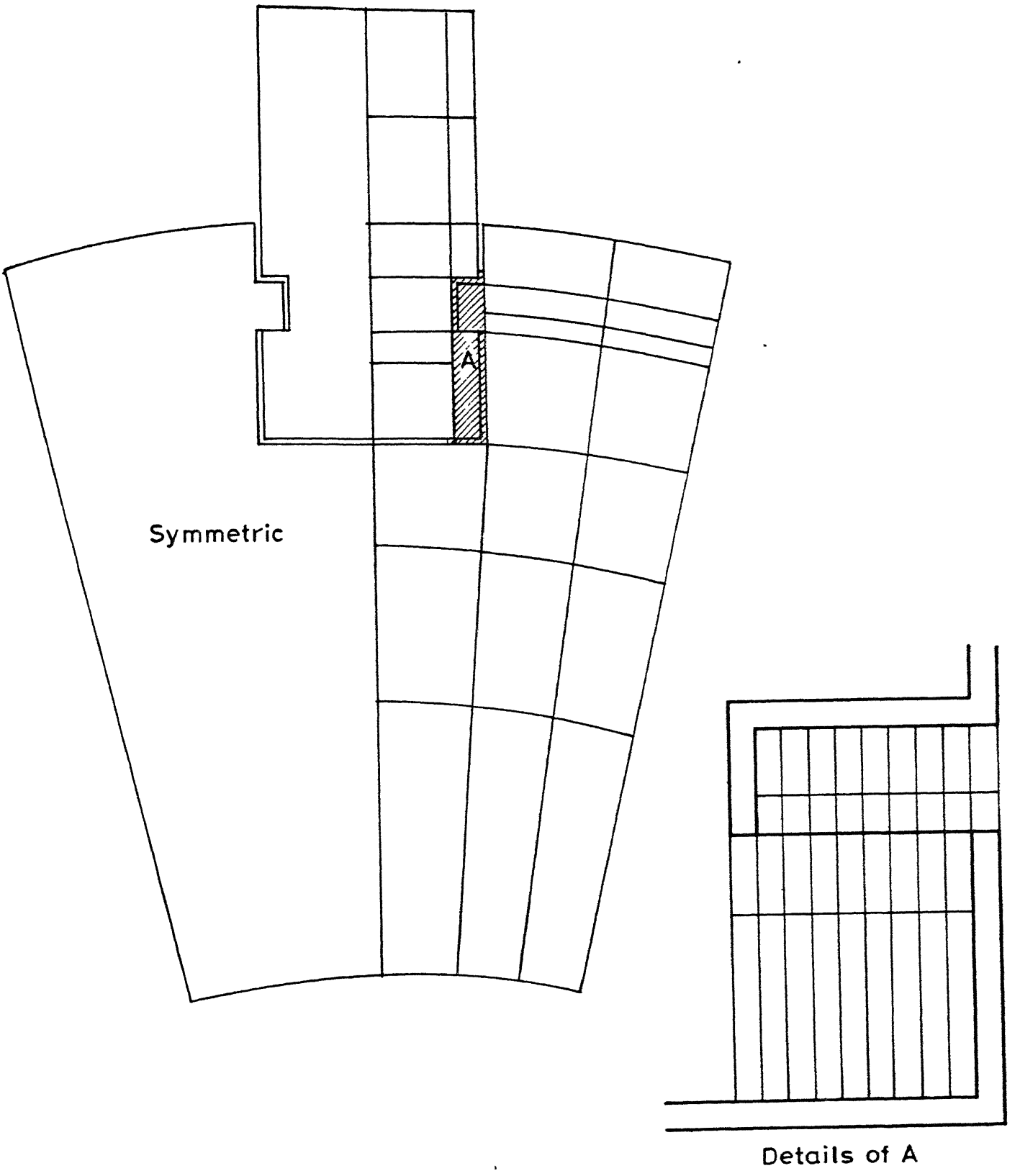

Fig. 3.12 Finite element mesh for the contact problem.

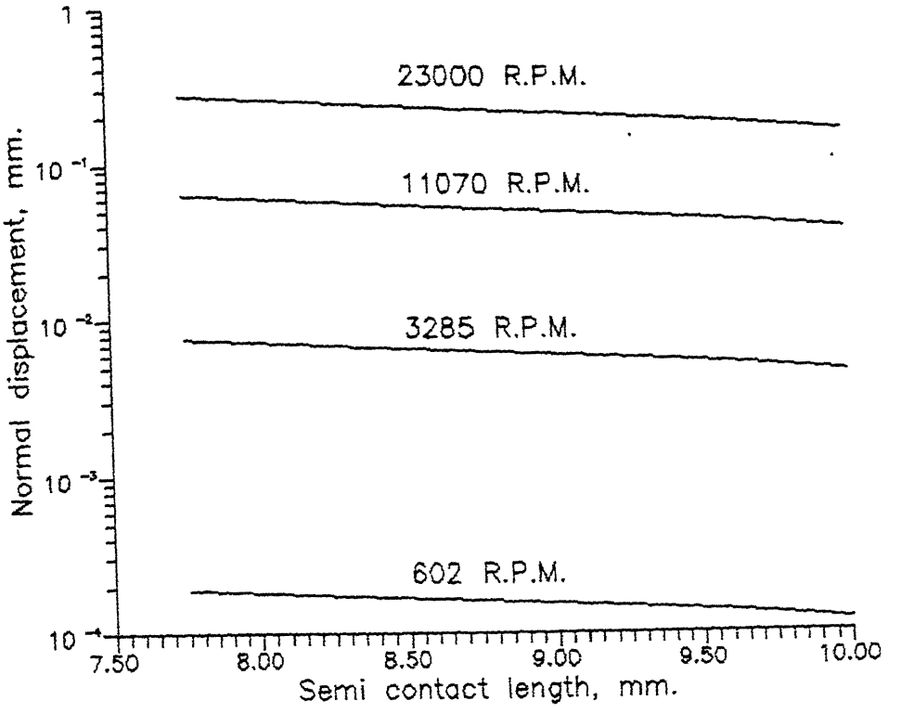

Fig 3.13(a) Variation of Normal Displacement along the Semi Contact Length for various Rotor Speeds (Mean Stress Boundary Condition)

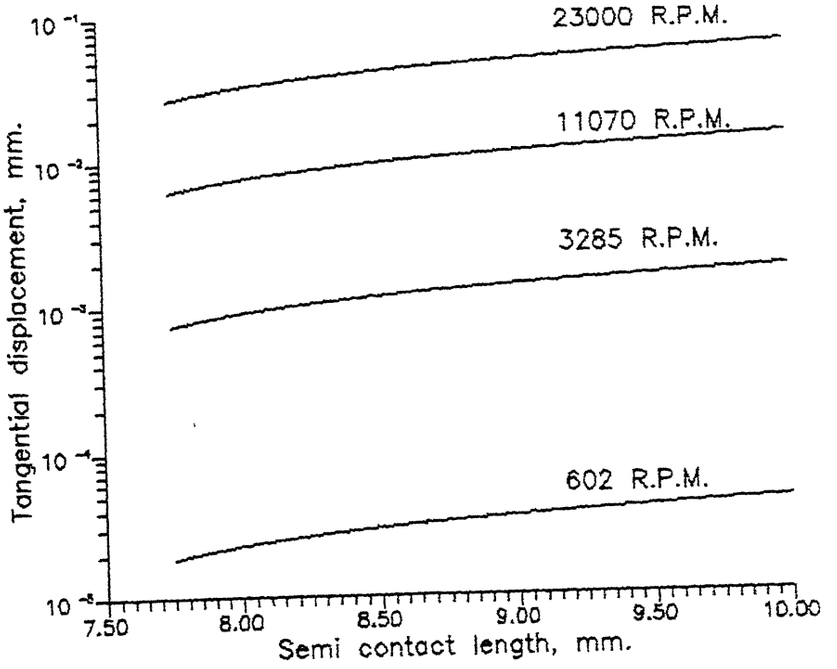

Fig 3.13(b) Variation of Tangential Displacement along the Semi Contact Length for various Rotor Speeds. (Mean Stress Boundary Condition)

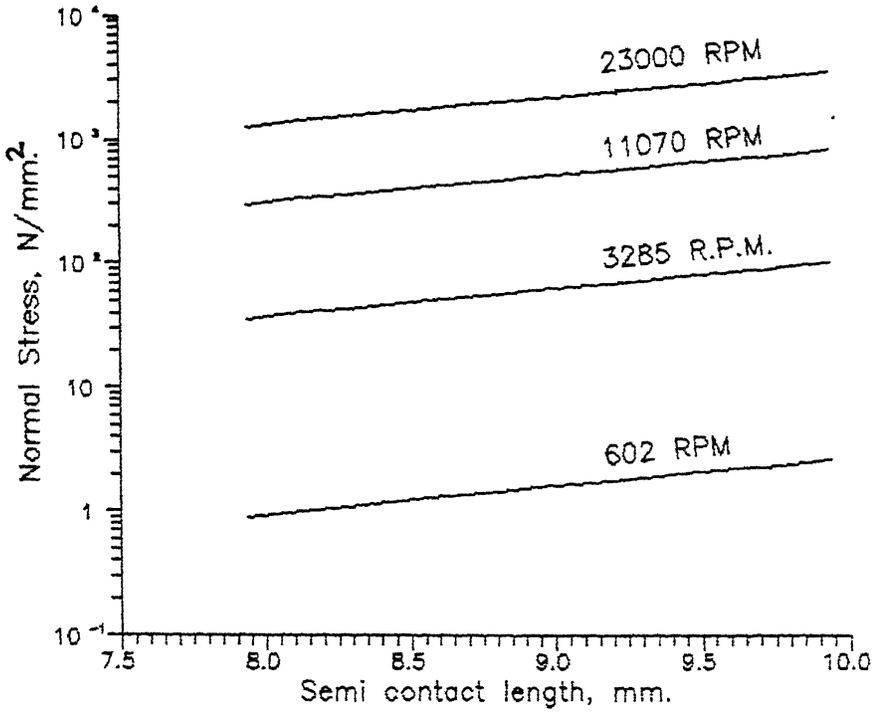

Fig 3.13(c) Variation of Normal Stress along the Semi Contact Length for variour Rotor Speeds. (Mean Stress Boundary Condition)

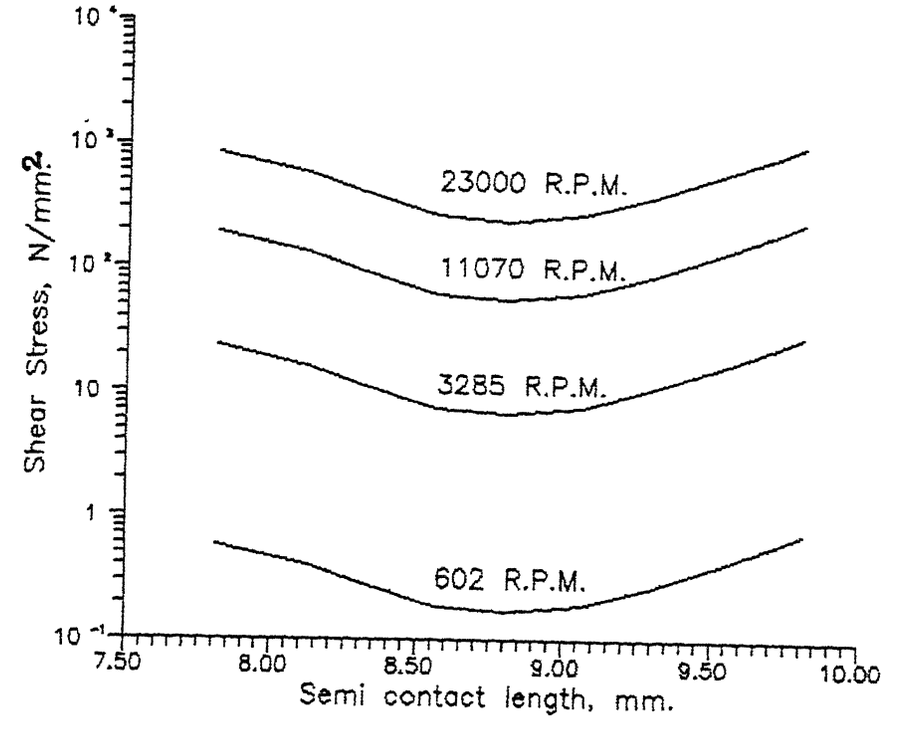

Fig 3.13(d) Variation of Shear Stress along the Semi Contact Length for various Rotor Speeds. (Mean Stress Boundary Condition)

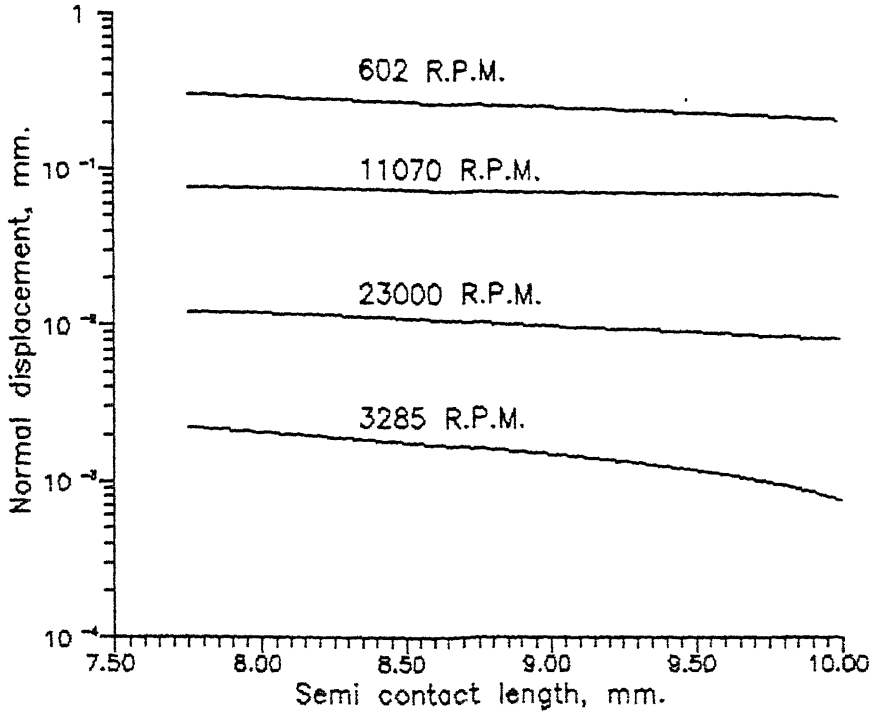

Fig 3.14(a) Variation of Normal Displacement along the Semi Contact Length for various Rotor Speeds. (Alternating Stress Boundary Condition)

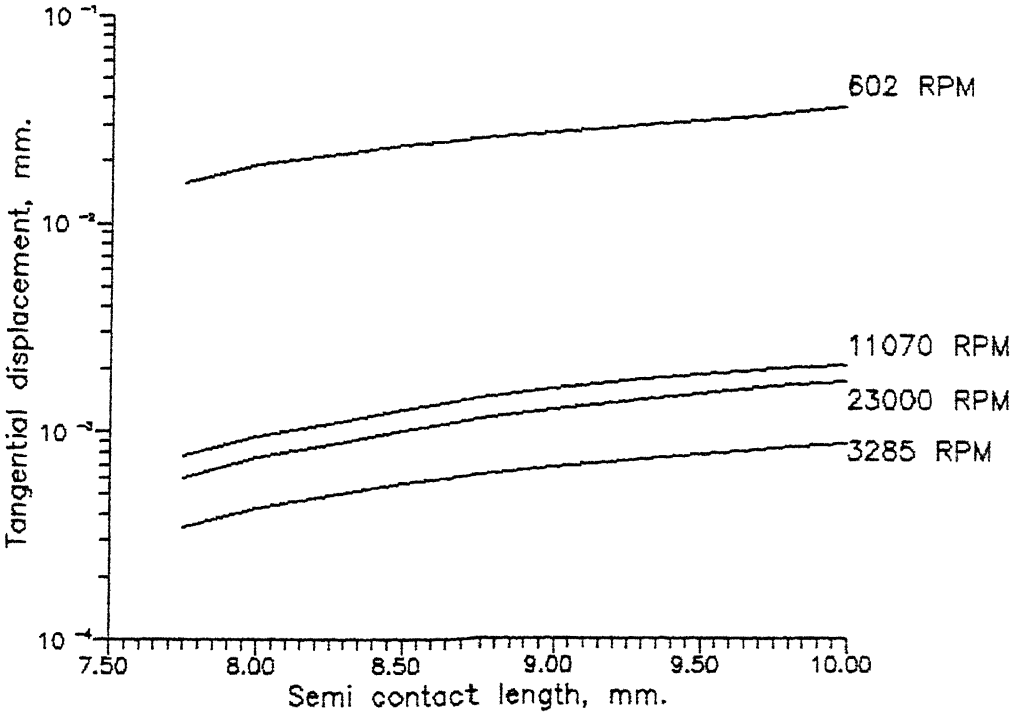

Fig 3.14(b) Variation of Tangential Displacement along the Semi Contact Length for Various Rotor speeds (Alternating Stress Boundary Condition)

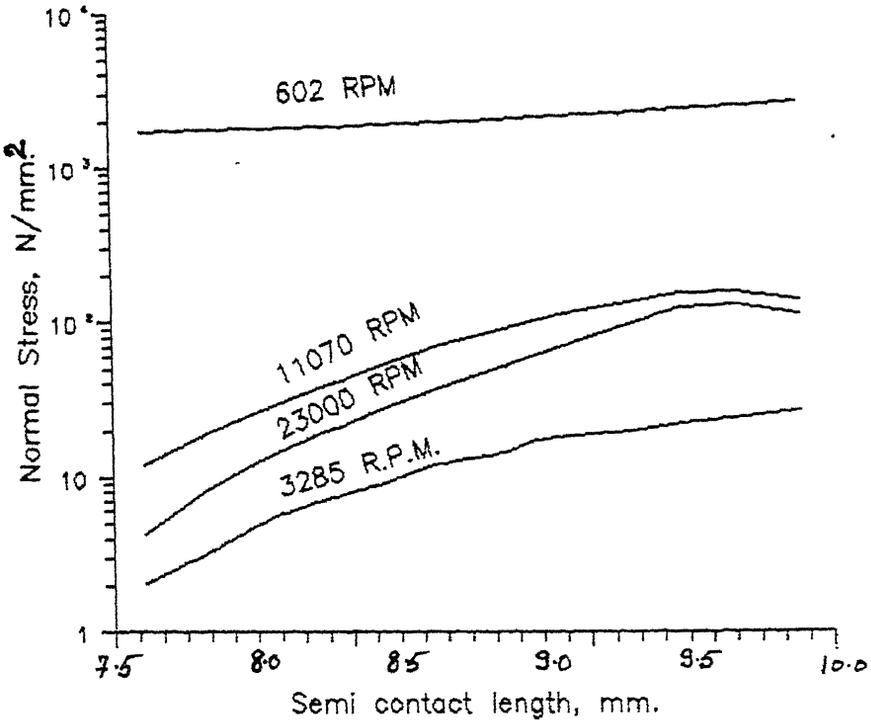

Fig 3.14(c) Variation of Normal Stress along the Semi Contact Length for various Rotor Speeds. (Alternating Stress Boundary Condition)

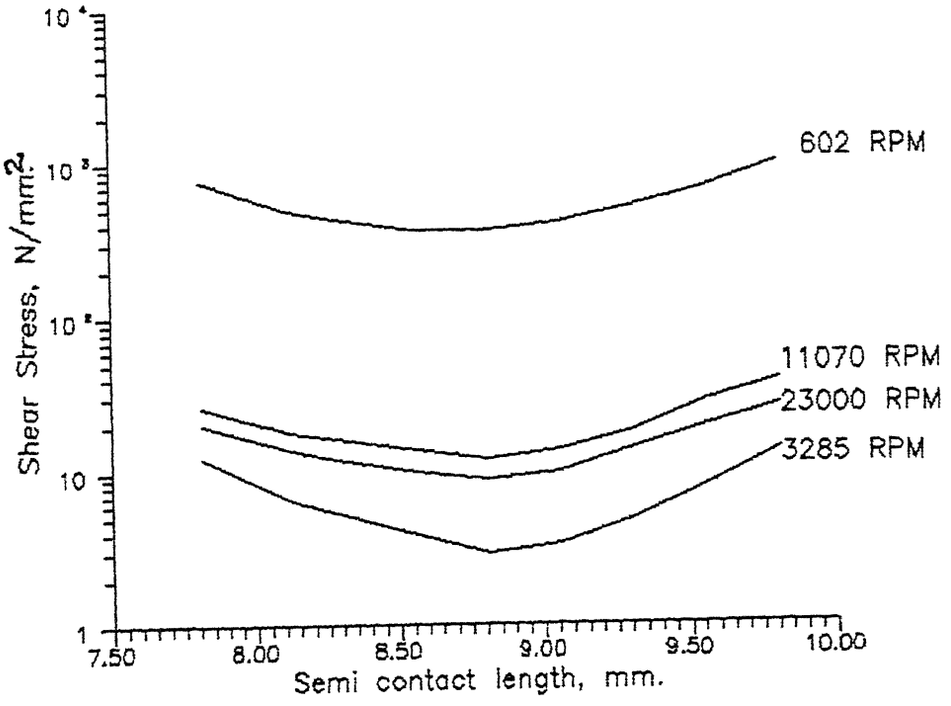

Fig 3.14(d) Variation of Shear Stress along the Semi Contact Length for various Rotor Speeds. (Alternating Stress Boundary Condition)

boundary conditions to the contact domain. It can be seen from these figures that the displacements and stresses increase all along the semi contact length with an increase in rotational speed. This is so because with the mean stress from the blade as a boundary condition, only centripetal forces due to rotation are being accounted for. Higher centripetal forces result in greater displacements and stresses at the contact interface. It can also be observed from these figures that at any particular rotor speed, the normal displacement of the semi contact interface is higher in the regions which are closer to Z-axis as compared to those in regions located farther from the Z-axis. On the other hand the normal stresses are lower in regions closer to Z-axis as compared to those in region farther from the Z-axis. This can be explained on the basis of the fact that the interlocking 'hook' *abcd* of the disc in Fig. 3.1 behaves somewhat like a cantilever experiencing a bending load from the blade root, allowing the blade root a greater displacement towards its 'free end' *bc* as compared to its fixed end *ad* and resulting consequently in lower stresses in regions towards *bc* as compared to those in regions closer to *ad*.

3.3.3.2 Alternating Contact Displacements and Stresses :

Similar trends at any particular rotor speed can be observed in Figs. 3.14 where the alternating stresses from the blade now form a boundary condition for the contact region. However in this case, unlike the results presented in Figs. 3.13, the stress and displacements values along the semi contact length need not necessarily increase with increasing rotor speed. The

stresses at any point on the semi contact length can be seen to be higher for a rotor speed of 6Ø2 RPM as compared to those at 3285 RPM. The RPM of 6Ø2 is a resonant rotor speed caused due to the interaction of the blade's first vibratory mode with the nozzle passing frequency. The resonance at 3285 RPM is caused due to the interaction of second vibratory mode with nozzle passing frequency. The alternating bending stresses on the section AB of the blade which is at a distance of 2Ø mm from the root (Fig. 3.1) are higher at 6Ø2 RPM as compared to those at 3285 RPM (refer Fig. 3.5). Hence these stresses which form the boundary conditions for the root domain bounded by AB and CDEF result in higher stresses at contact interface ba for 6Ø2 RPM and lower stresses for 3285 RPM.

From the beam theory the maximum stress at the root is found to be 94Ø N/mm^2 (Fig.3.5) while its value is 3Ø25 N/mm^2 when the root region is analysed as a contact problem (Fig. 3.14). The above difference in stresses clearly emphasizes the need for the analysis of the contact region. On the basis of the analysis and results presented, it is possible now to obtain the mean and alternating stresses at the blade-disc root interface. The vulnerable regions of the interface can thus be identified. The mean and alternating stresses would form the two axis of the mean stress diagram (i.e. Goodman diagram) to predict the fatigue damage and residual life of the vulnerable interfacial zones.

3.3.3.3 Parametric Study :

A study was further carried out to examine the effect of variation of X and Z clearances, at the blade root junction (See Fig. 3.1), on the interfacial stresses and displacements. The variation in the clearances is caused either by

(i) keeping the disc dimensions fixed and varying the blade dimensions.

or by

(ii) keeping the blade dimensions fixed and varying the disc dimensions.

These results in terms of displacements and stresses for the entire semi contact length are presented in Fig. sets 3.15 - 3.18 for various X and Z clearances. To display the trends more clearly the variation of the stresses and displacements at the mid-node alone of the semi contact length with variation in X and Z clearances are presented in Fig. sets 3.19 and 3.2Ø. The effect of once keeping the blade dimension fixed and then keeping the disc dimensions fixes is presented simultaneously on the same graph.

Starting with an initial set of X and Z clearances (Ø.25 mm. and Ø.25 mm. respectively). Figs. 3.19 and 3.2Ø depict the effect of reduction in clearances. It can be seen that a reduction in X clearance 'in general' leads to a reduction in the contact displacements and normal stresses. This is so for a reduction in X clearance implies either an increase in blade root cross-section area fb (when disc dimensions are fixed) or an increase in contact area ba shown in Fig. 3.1 (when the blade

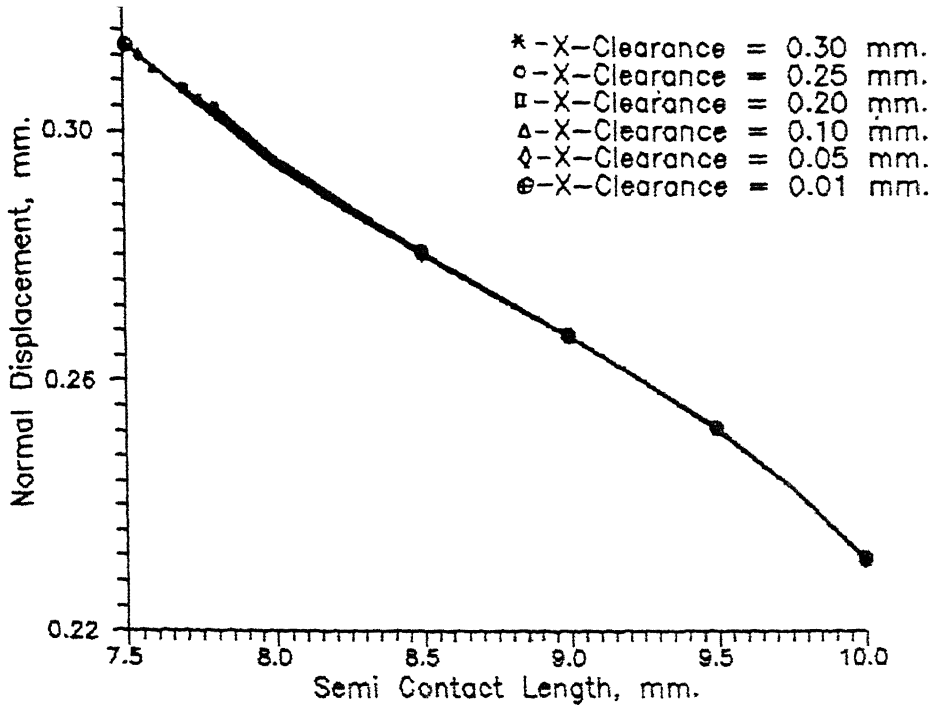

Fig 3.15(a) Variation of Normal Displacement along the Semi Contact Length for Various Values of X Clrarences. (Blade Dimensions Fixed). Rotor Speed = 602 RPM.

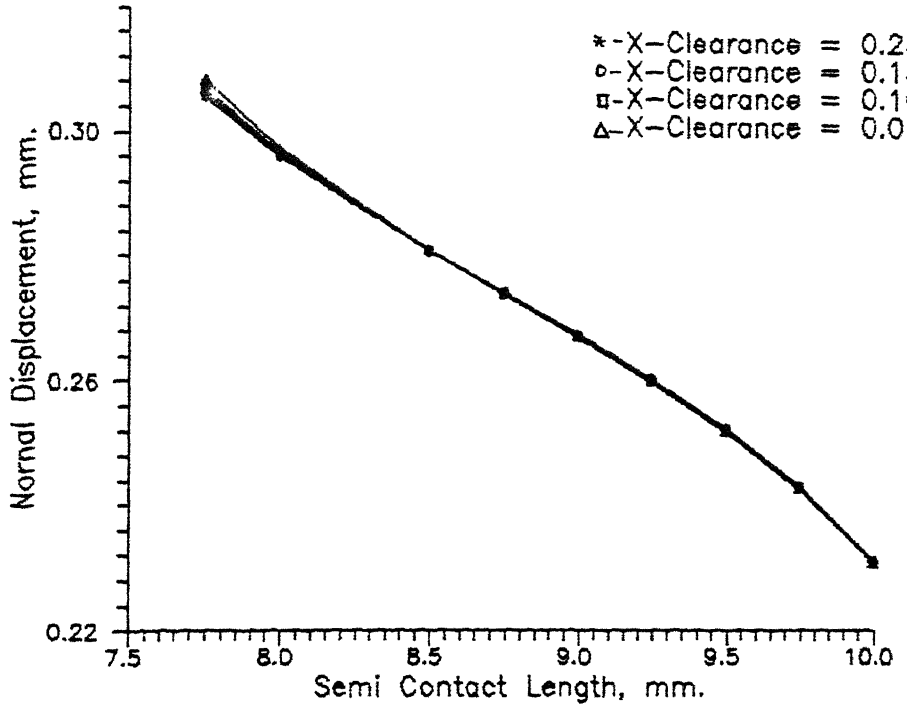

Fig.3.15(b) Variation of Normal Displacenemt along the Semi Contact Length for various values of X Clearances. (Disc Dimentions Fixed). Rotor Speed = 602 RPM.

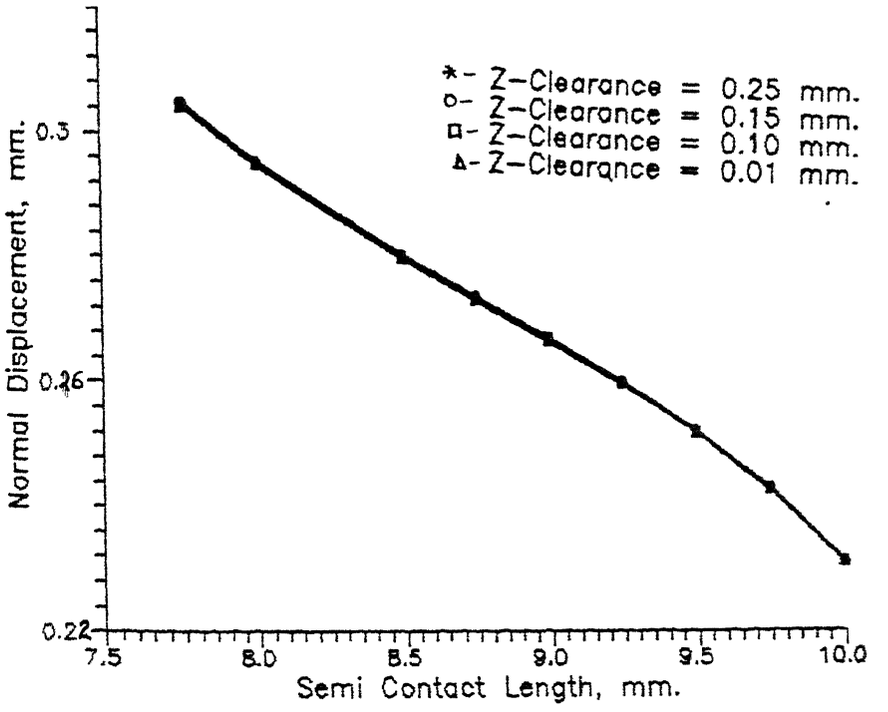

Fig.3.15(c) Variation of Normal Displacement along the Semi Contact Length for various values of Z Clearances. (Blade Dimensions Fixed). Rotor Speed = 602 RPM.

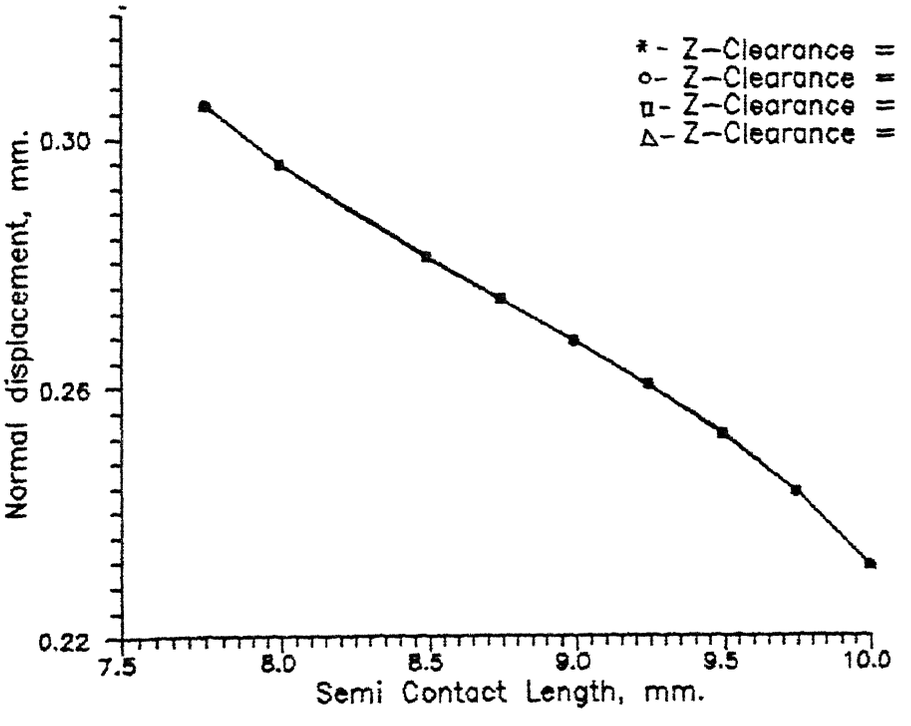

Fig.3.15(d) Variation of Normal Displacement along the Semi Contact Length for various Values of Z Clearances. (Disc Dimensions Fixed) Rotor Speed = 602 RPM.

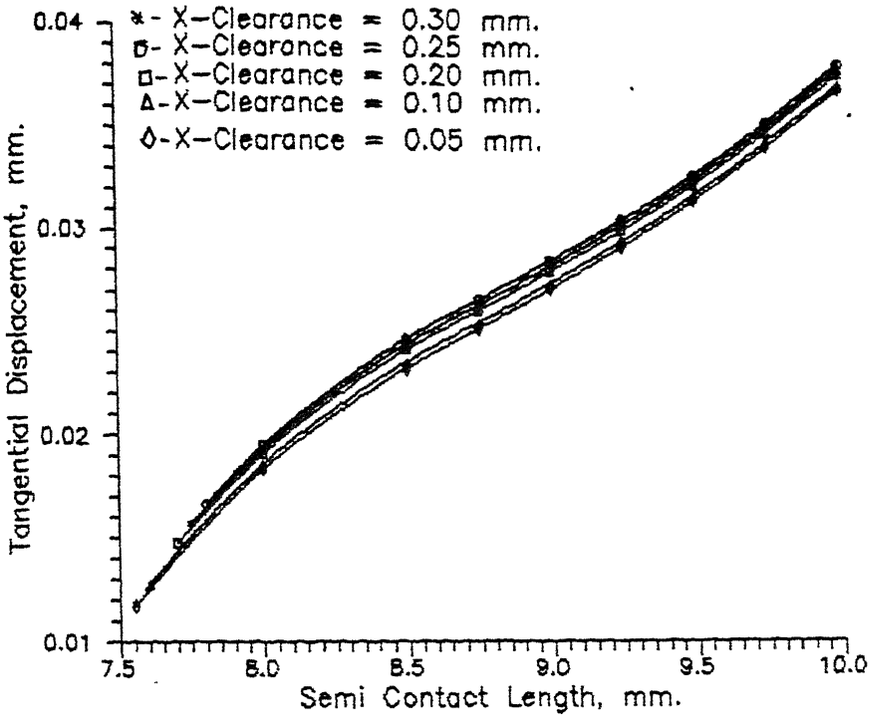

Fig.3.16(a) Variation of Tangential Displacement along the Semi Contact Length for various Values of X Clearances. (Blade Dimensions Fixed). Rotor Speed = 602 RPM.

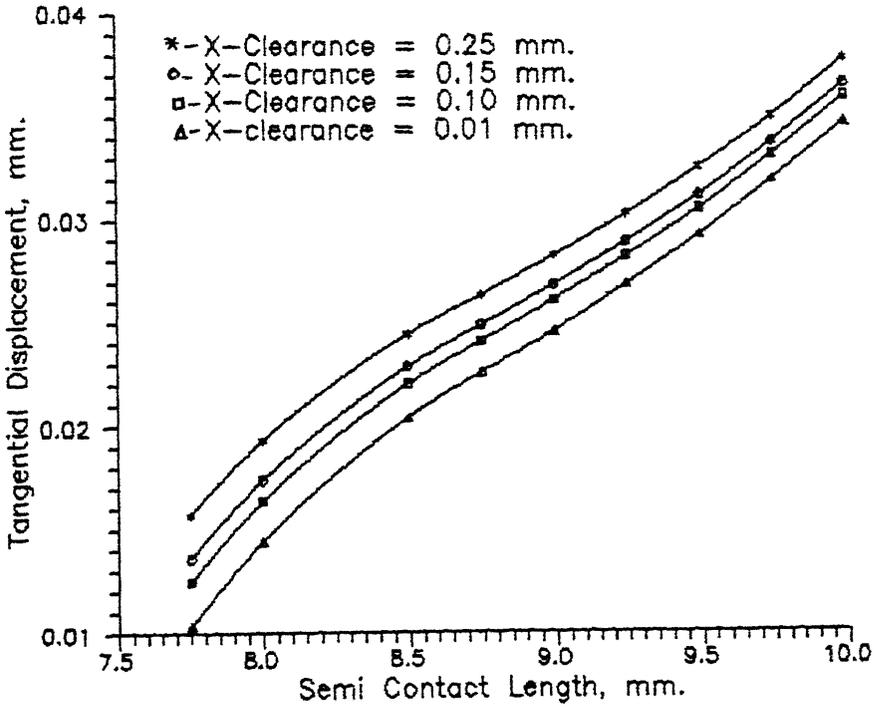

Fig.3.16(b) Variation of Tangential Displacement along the Semi Contact Length for various Values of X Clearances. (Disc Dimensions Fixed). Rotor Speed = 602 RPM.

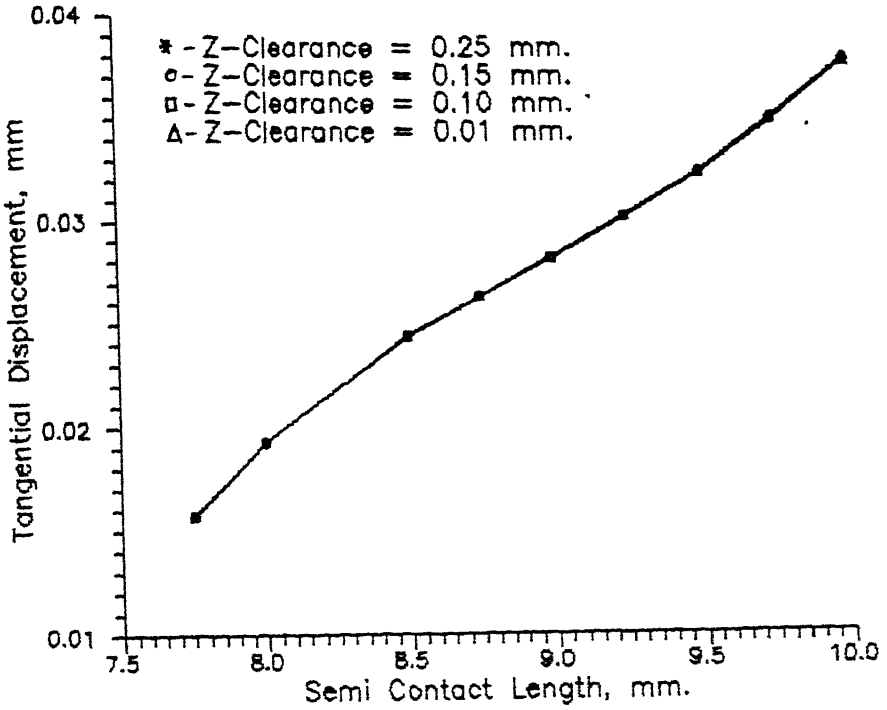

Fig.3.16(c) Variation of Tangential Displacement along the Semi Contact Length for various Values of Z Clearances. (Blade Dimensions Fixed). Rotor Speed = 602 RPM.

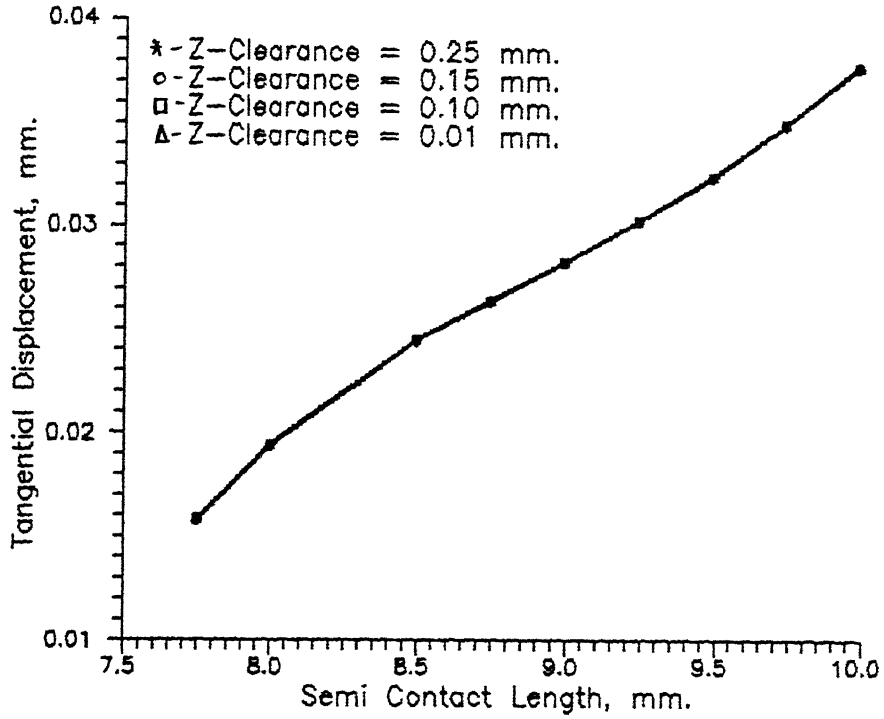

Fig.3.16(d) Variation of Tangential Displacemant along the Semi Contact Length for various Values of Z Clearances. (Disc Dimensions Fixed). Rotor Speed = 602 RPM.

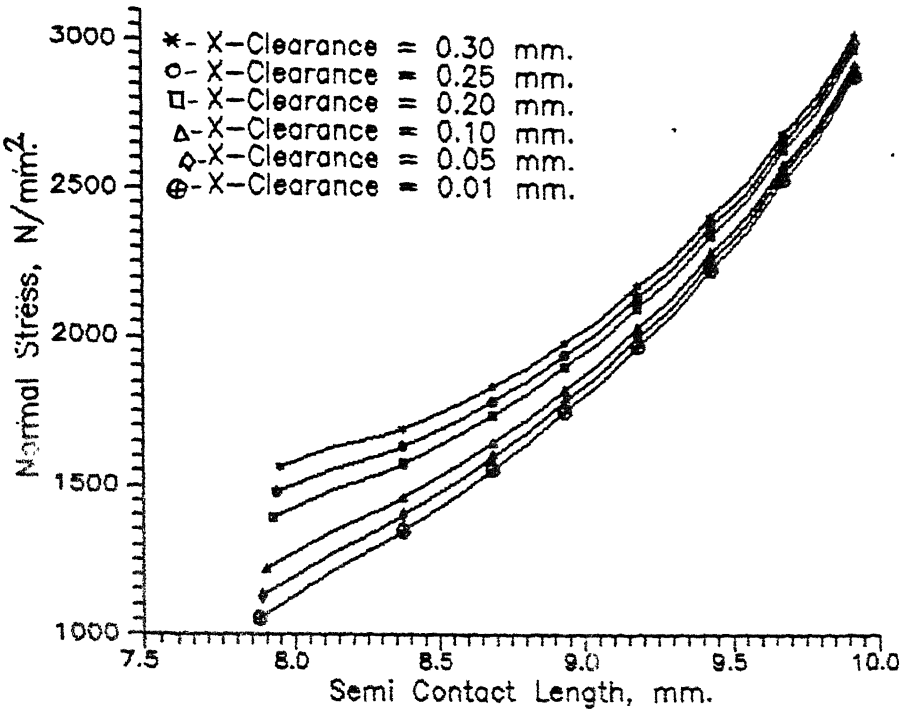

Fig 3.17(a) Variation of Normal Stress along the Semi Contact Length for various Values of X Clearances (Blade Dimensions Fixed). Rotor Speed = 602 RPM.

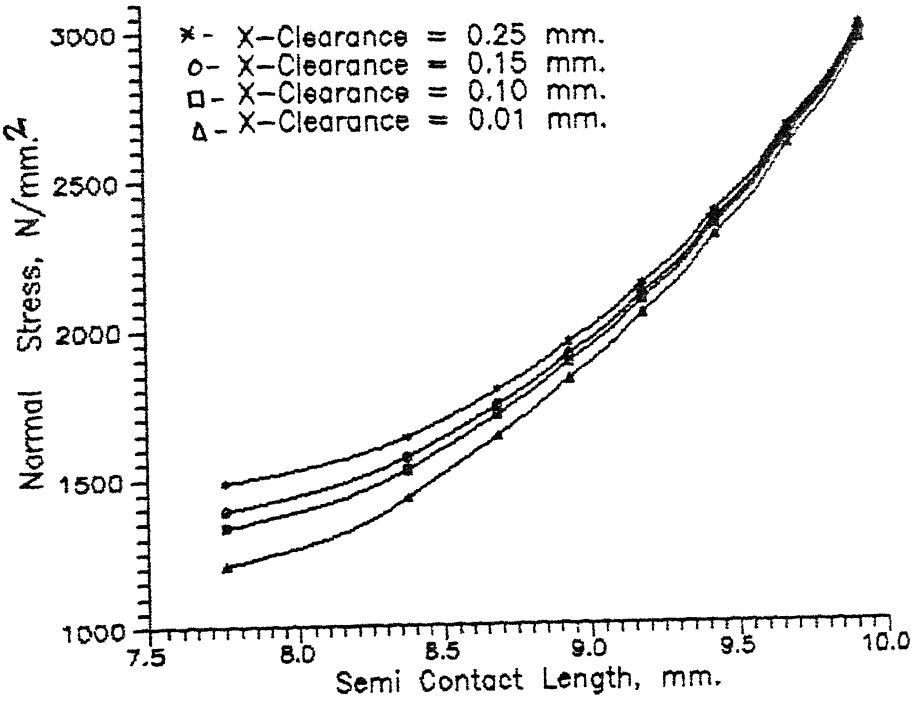

Fig 3.17(b) Variation of Normal Stress along the Semi Contact Length for various Values of X Clearances. (Disc Dimensions Fixed). Rotor Speed = 602 RPM.

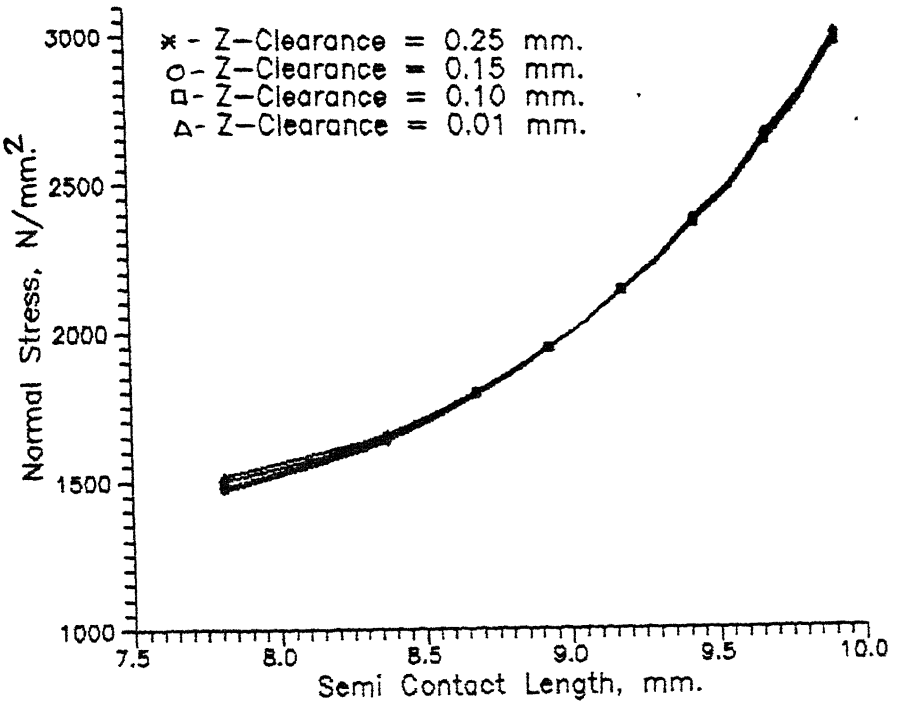

Fig 3.17(c) Variation of Normal Stress along the Semi Contact Length for various Values of Z Clearances. (Blade Dimensions Fixed). Rotor speed = 602 RPM.

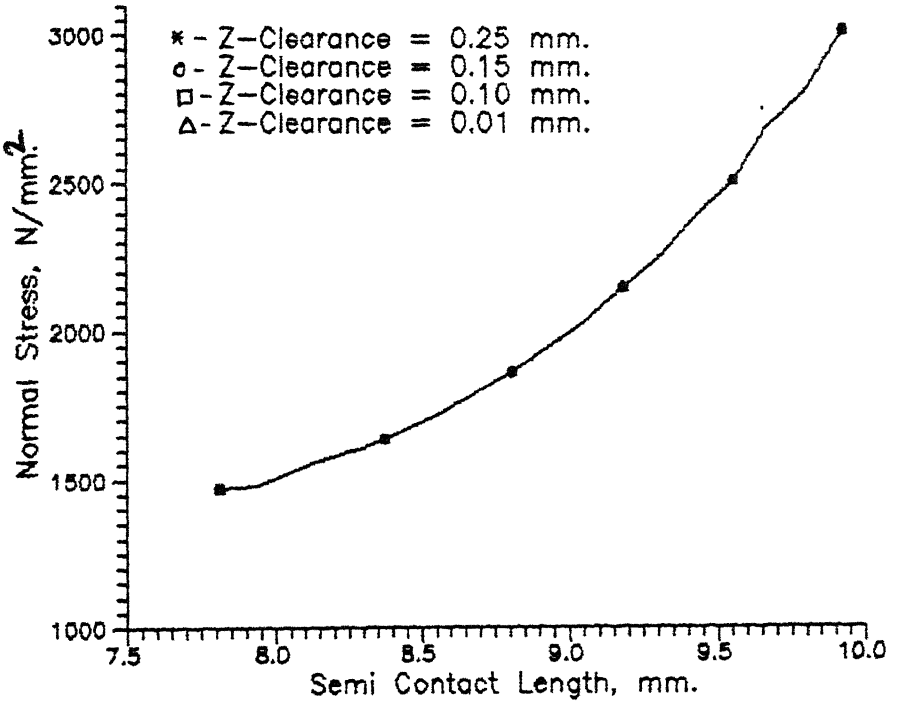

Fig 3.17(d) Variation of Normal Stress along the Semi Contact Length for various Values of Z Clearances. (Disc Dimensions Fixed). Rotor Speed = 602 RPM.

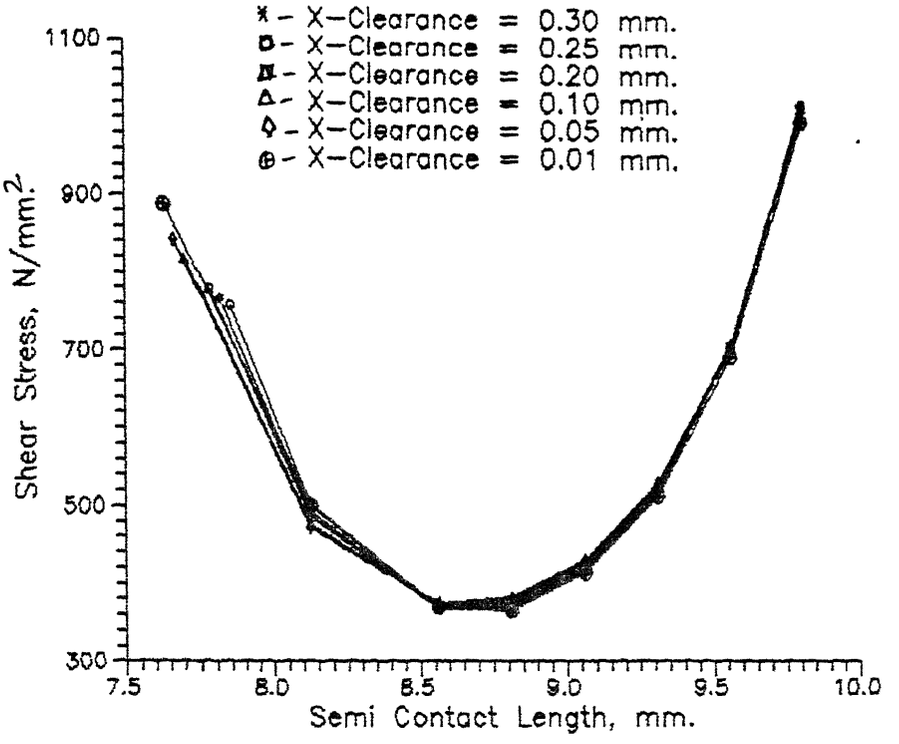

Fig.3.18(a) Variation of Shear Stress along the Semi Contact Length for various Values of X Clearances. (Blade Dimensions Fixed). Rotor Speed = 602 RPM.

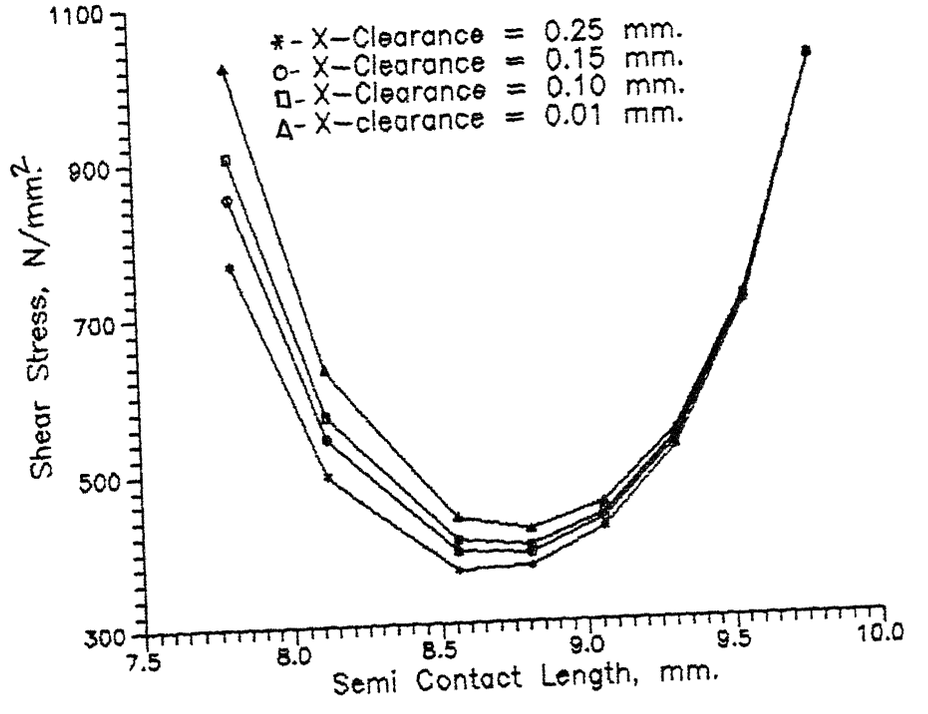

Fig.3.18(b) Variation of Shear Stress along the Semi Contact Length for various values of X Clearances. (Disc Dimensions Fixed). Rotor Speed = 602 RPM.

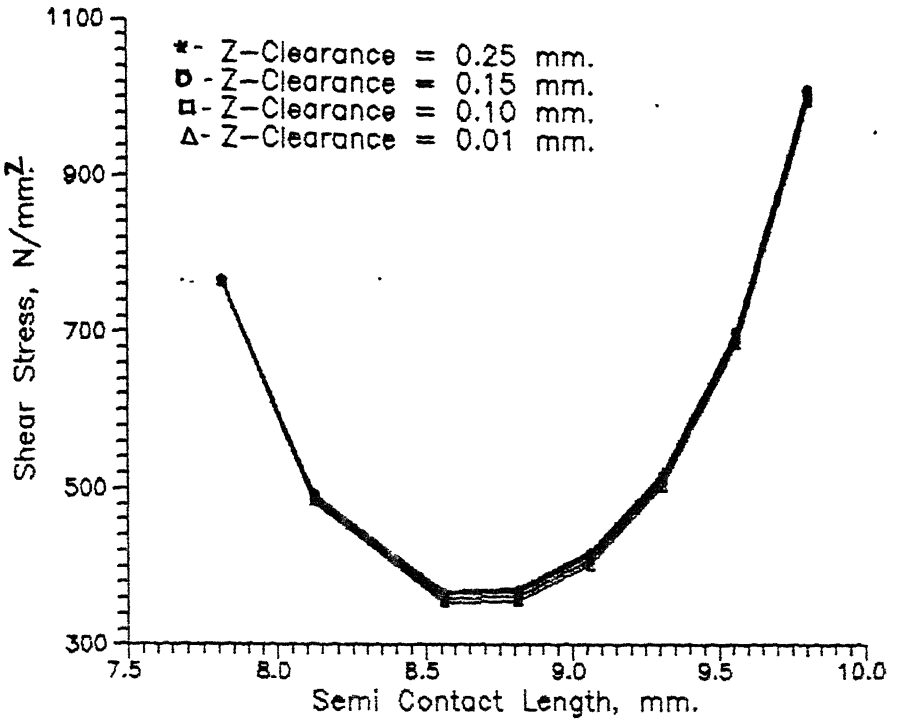

Fig.3.18(c) Variation of Shear Stress along the Semi Contact Length for various Values of Z Clearances. (Blade Dimensions Fixed). Rotor Fixed = 602 RPM.

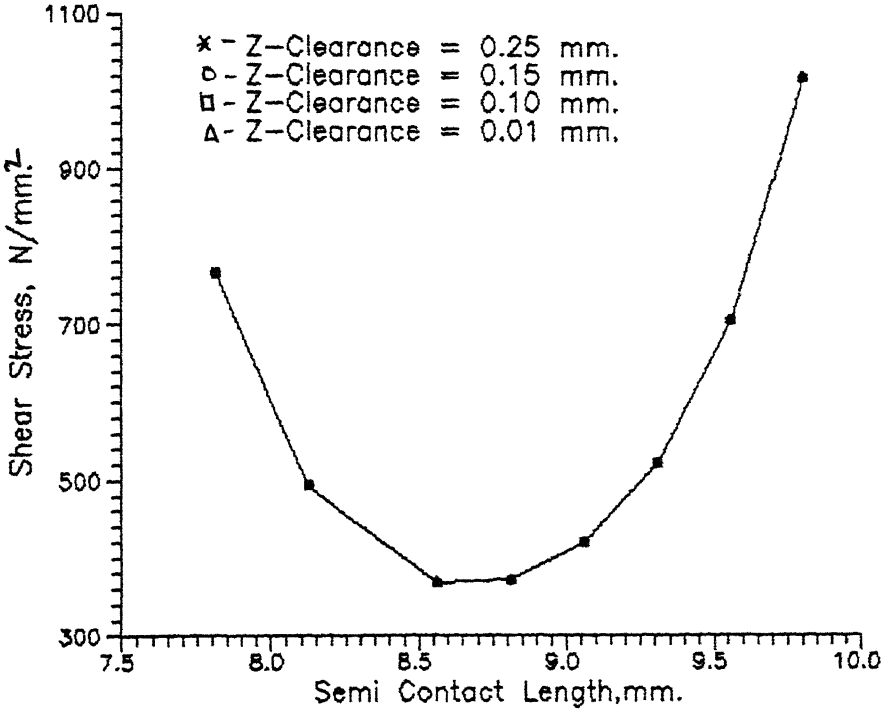

Fig.3.18(d) Variation of Shear Stress along the Semi Contact Length for various Values of Z Clearances. (Disc Dimensions Fixed). Rotor Speed = 602 RPM.

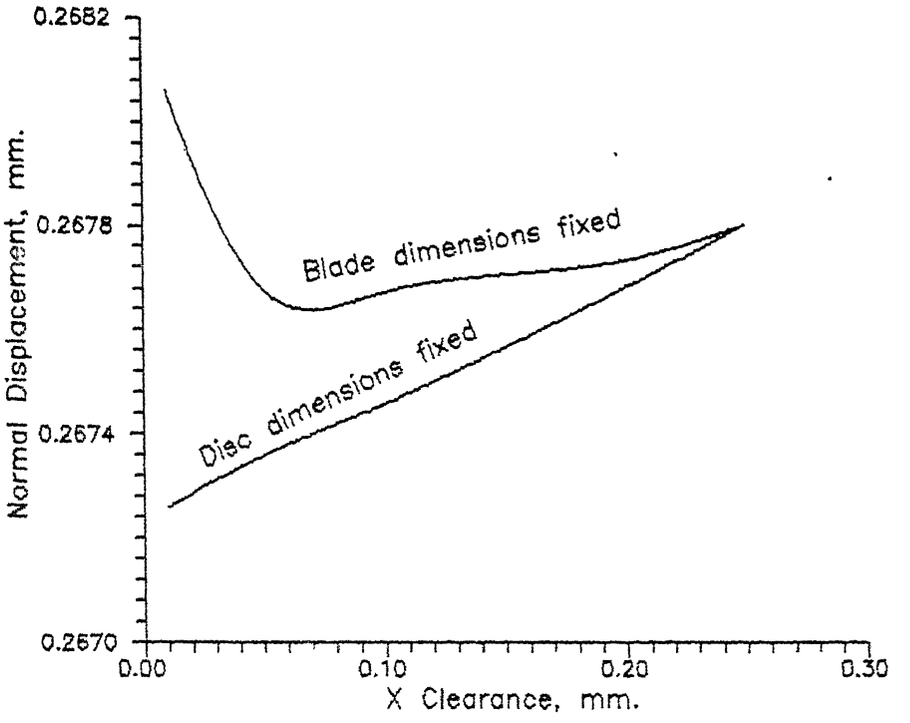

Fig.3.19(a) Variation of Normal Displacement at the Mid-Node of the Semi Contact Length against X Clearance.

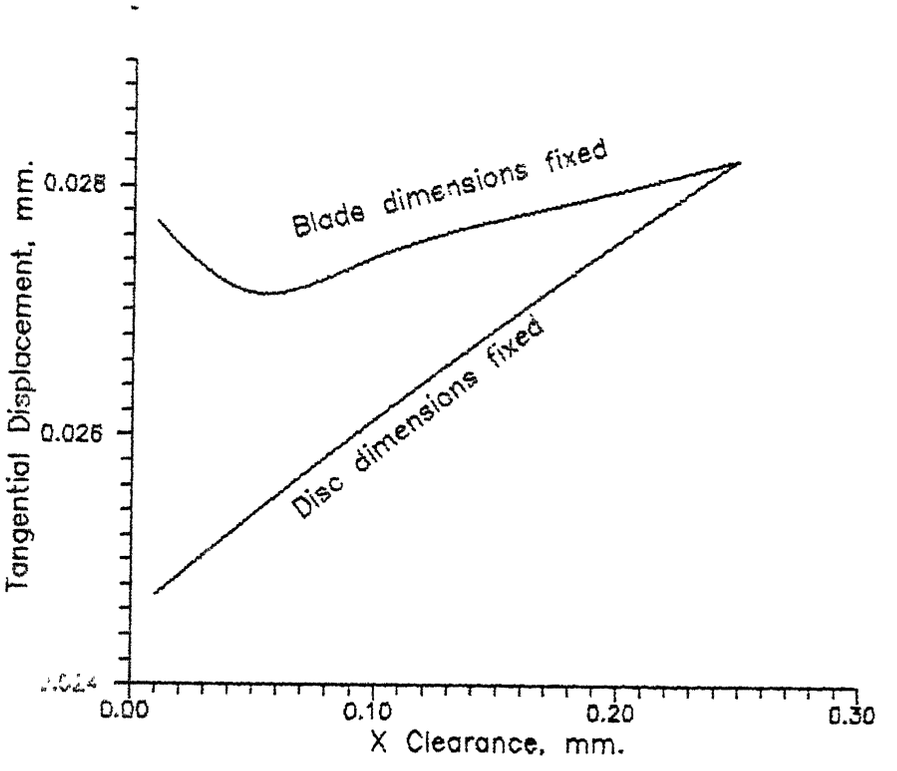

Fig.3.19(b) Variation of Tangential Displacement at the Mid-Node of the Semi Contact Length against X Clearance.

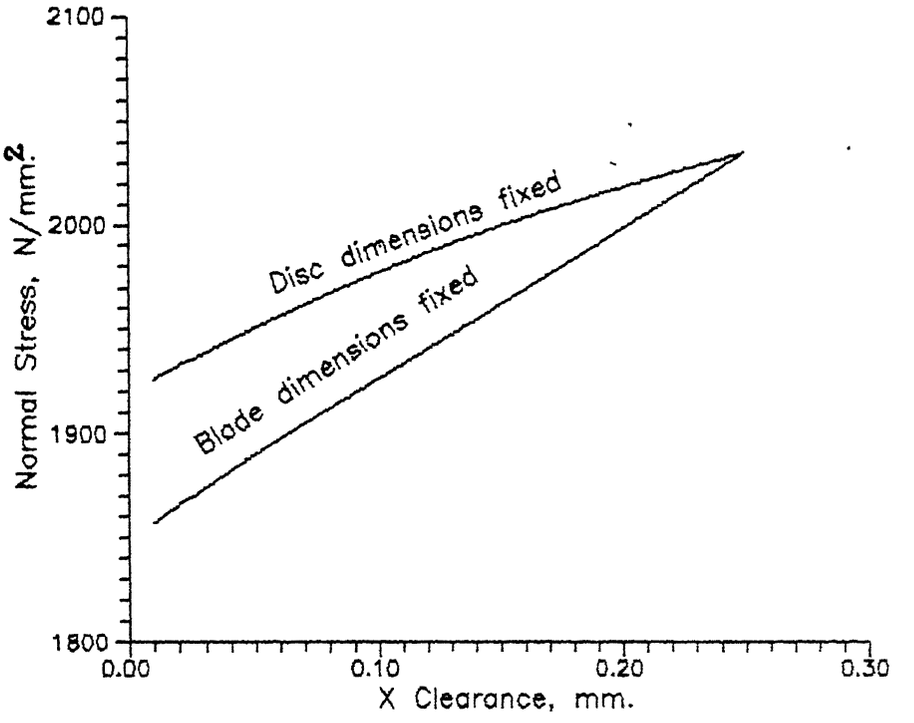

Fig.3.19(c) Variation of Normal Stress at the Mid-Node of the Semi Contact Length against X Clearance.

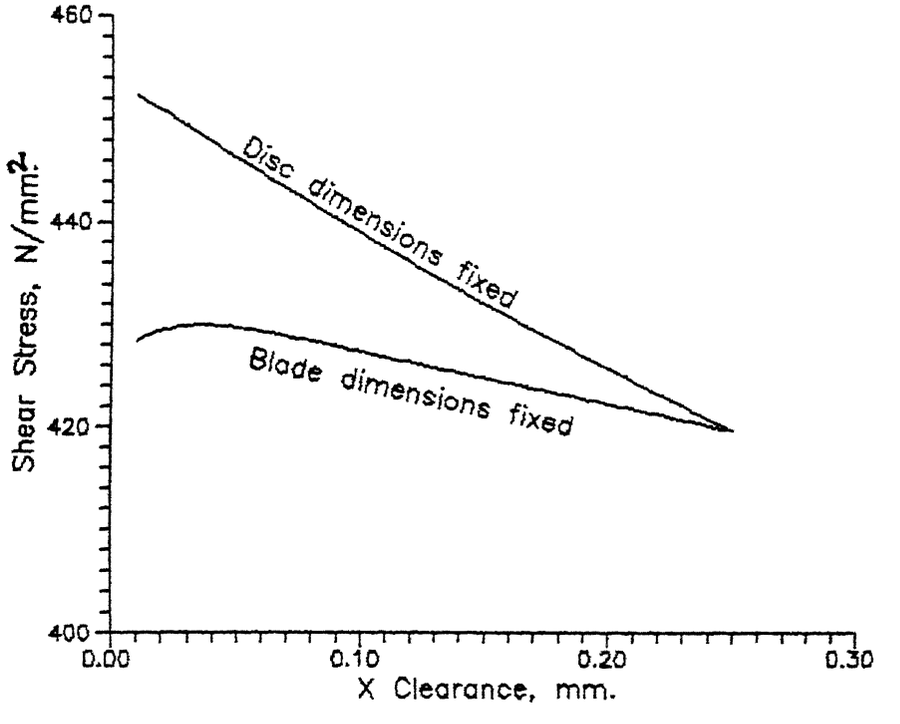

Fig.3.19(d) Variation of Shear Stress at the Mid-Node of the Semi Contact Length against X Clearance.

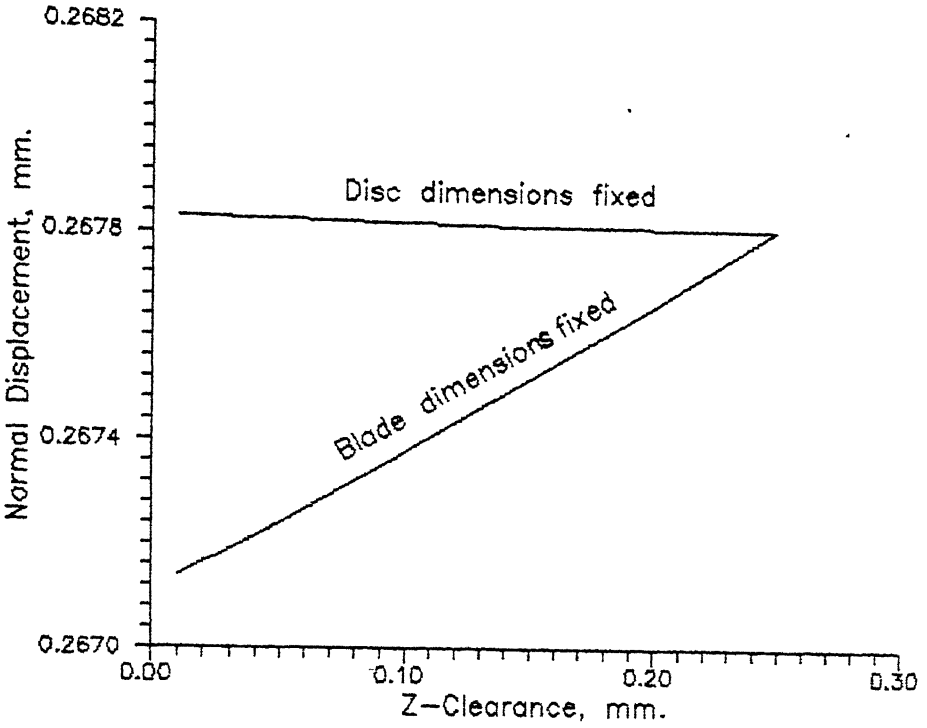

Fig.3.20(a) Variation of Normal Displacement at the Mid-Node of the Semi Contact Length Against Z Clearance.

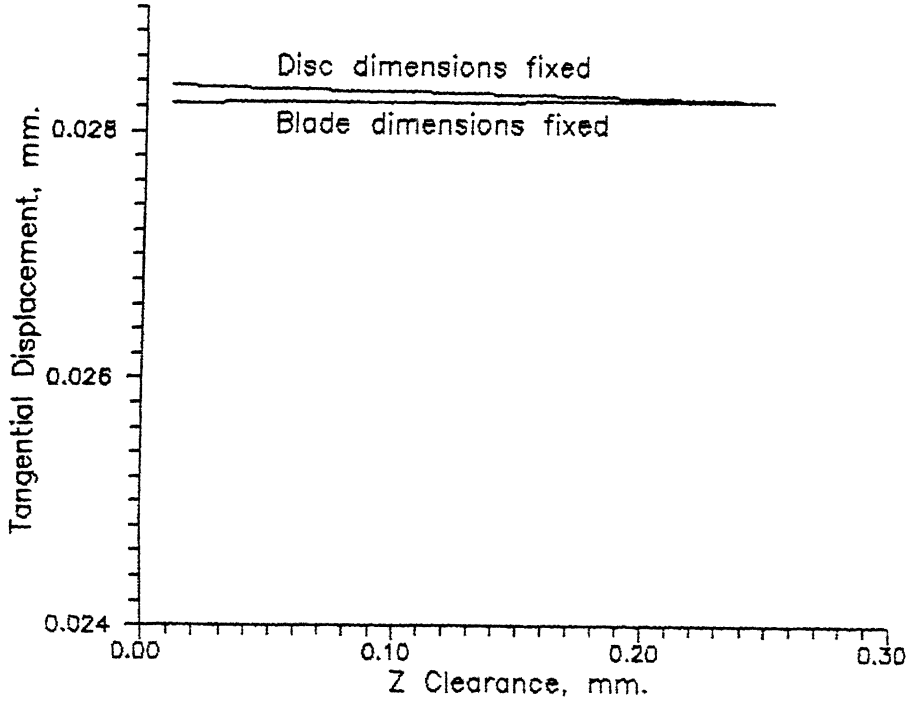

Fig.3.20(b) Variation of Tangential Displacement at the Mid- of the Semi Contact Length against Z Clearance.

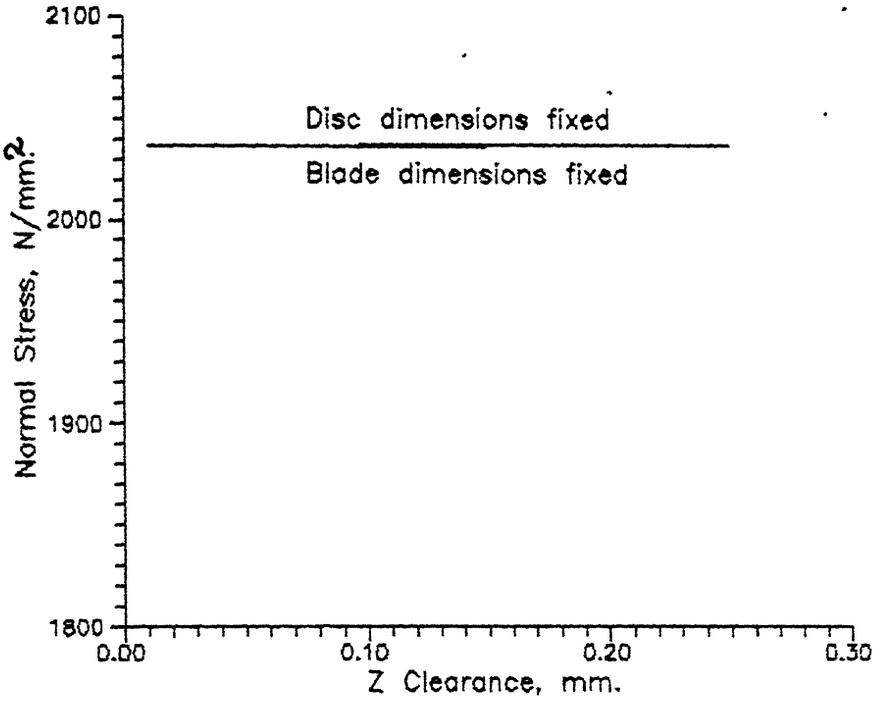

Fig.3.20(c) Variation of Normal Stress at the Mid-Node of the Semi Contact Length against Z Clearance.

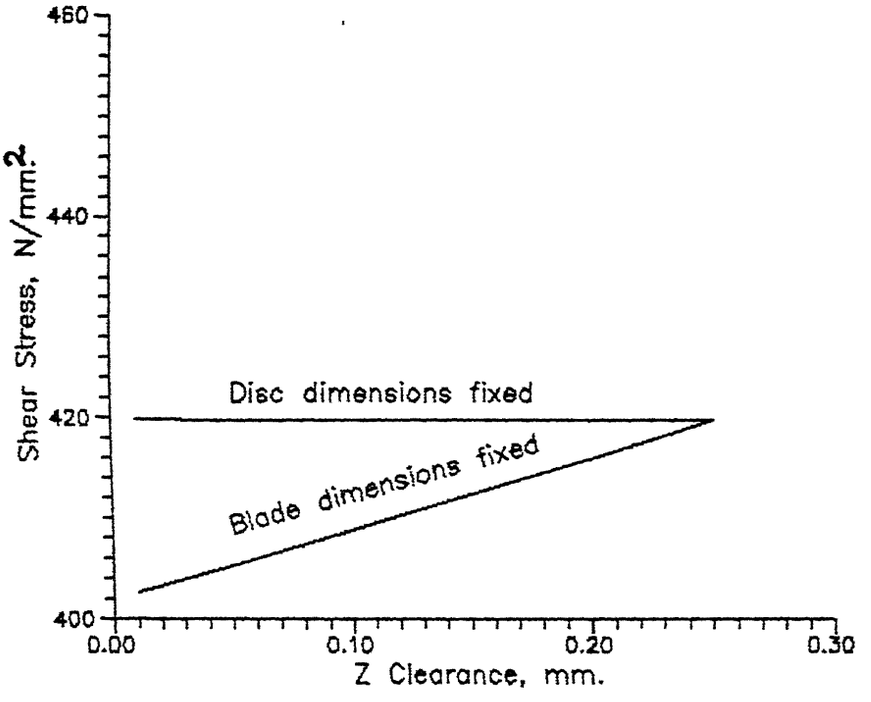

Fig.3.20(d) Variation of Shear Stress at the Mid-Node of the Semi Contact Length against Z Clearance.

dimensions are fixed). Both result in an increase in load bearing capacity consequently causing reduction in the interfacial displacements and normal stresses. It can also be seen that the increase in load bearing capacity is more prominent when the contact area *ba* is increased as compared to an increase in the blade cross-sectional area at *fb*. It can be seen however that after a certain point an increase in the contact area *ba* (by varying the disc dimensions) results in increased displacement. This can be explained on the basis of the fact that an increase in contact area *ba* also implies a reduction of stiffness of the cantilevered 'hook' *abcd*. Stiffness reduction becomes more prominent after a certain point whilst increasing the contact area for increasing load bearing capacity.

With the decrease in Z clearance by changing the disc groove dimension, the stiffness of the 'hook' *abcd* increases which causes decrease in the normal displacement. But the stresses remain unchanged. If Z clearance is varied by varying blade root dimensions, there is no appreciable change in displacement or stresses.

It is realized that a more detailed parametric analysis and consideration of different types of roots (e.g. Firtree, Dovetail etc.) is essential to gain more meaningful insights.

However the present study does underline the relevance of such future work, if undertaken.

CHAPTER IV

CONCLUSIONS AND SUGGESTIONS FOR FUTURE WORK

The general computer program developed in chapter three determines

(i) the natural frequencies, mode shapes and the displacements and stresses as functions of the blade coordinate for various rotor speeds,

(ii) the radial and circumferential stresses as functions of the radial coordinate for various rotor speeds, and

(iii) the normal and tangential displacements and the normal and shear stresses along the contact surface for various values of the following two parameters

(a) rotor speed, and (b) domain clearances.

Based on these results following conclusions can be drawn.

(i) From the beam theory, the maximum stresses at the root is found to be 94Ø N/mm^2 while its value is 3Ø25 $N/mm.^2$ when the root region is analysed as a contact problem. There is an increase in the maximum root stress by about 3ØØ % . This difference is clearly emphasizes the need for the analysis of the root region as a contact problem.

(ii) For mean stress boundary condition, the contact displacements and stresses increase with the rotor speed. On the other hand, for the alternating stress boundary condition, there is no such simple trend. Here the variation with respect to rotor speed

depends on the dominant mode of vibration.

(iii) 'In general', the reduction in X clearance leads to a reduction in the contact displacements and the normal stresses. This reduction is more prominent when the clearance is reduced by keeping the blade dimensions fixed. Comparatively, the change in Z clearance has a very little effect on the contact displacements and stresses.

As mentioned in chapter one, this work has several limitations in the form of idealizations made and methodologies used. In future, some or all of these can be accounted for. In particular the following modifications can be undertaken :

(i) In the analysis of the blade, the actual geometry of the blade should be considered. It means the effects of taper, twist, the asymmetry of the cross-section and the aspect ratio should be accounted for. [6]

(ii) Because of the finite number of blades and the change in geometry resulting from the grooves, the disc should not be considered as an axisymmetric body. Instead, its typical sector should be analysed as a plane stress problem.

(iii) Instead of treating a small layer of the contact region as a plane stress problem, the whole of it should be analysed as a 3-D Problem. Further the boundary of the domain should be chosen such that it has no effects on the contact displacements and stresses. The energy loss due to friction also has to be accounted for. Finally, for transient problems, the incremental loading procedure should be adapted.

REFERENCES

1. Dewey R.P. and Rieger N.F., " Survey of Steam Turbine Blade Failure ", Proc. EPRI Workshop on Steam Turbine Reliability , Boston, MA. , 1982

2. Rao J.S. and Vyas N.S., "Application of Reissner Method to Free Vibration of A Tapered, Twisted ,Aerofoil Cross-sectional Blade ", Defence Sci. J., Vol-36, No. 3, Page 273, 1986.

3 Sisto F. and Chang A.T., "A Finite Element Method for Vibration Analysis of Twisted Blades Based on Beam Theory ", AIAA J, Vol-422, Page 1646, 1984.

4 Leissa A.W., Macbain J.C. and Kielb R., "Vibration of Twisted Cantilever Plates : Summary of Previews and Current Studies ", Sound and Vib. J., Vol-96, No. 2, Page 159, 1984.

5 Rao J.S., Gupta K. and Vyas N.S., "Blade Damping Measurement in A Spin Rig with Nozzle Excitation Simulated by Electromagnets ", The Shock and Vibration Bulletin, Pt-2, Page 1Ø9, 1986.

6 Rao J.S. and Vyas N.S., "On Life Estimation of Turbine Blading ", 7th IFToMM World Conference, Sevilla, Spain, September 1987.

7. Rieger N.F. and Nowak W.J., "Analysis of Fatigue Stress in Turbine Blade Groups ", EPRI Seminar on Steam Turbine Availability, Palo Alto, CA, 1977

8. Matsura T., "Blade Bending Vibrations Induced by Wakes ", JMES, Vol-21, Page 136, 1978.

9. Hoyniak D. and Fleeter S., "Prediction of Aerodynamically Induced Vibrations in Turbomachinary ", ASME Winter Annual Meeting., Page 1, 1981.

1Ø. Gladwell G.M.L., " Contact Problems in the Classical Theory of Elasticity " , Sijithoff and Nordhoff, The Netherlands, 1973.

11. Muskhelishvili N.I., "Some Basic Problems of the Mathematical Theory of Elasticity ", 4th edition, Nordhoff International Pub., Leyden, 1954.

12. Chan S.K. and Tuba I.S., "A Finite Element Method for Contact Problems of Solid Bodies ", Part-I, Theories and Validation., Int. J. Mech. Sci., Vol-13, Page 615-625, 1971.

13. Ohte S., "Finite Element Analysis of Elastic Contact Problems ", Bulletin of JSME, Vol-16, Page 797-8Ø8, 1973

14. Francavilla A. and Zienkiewicz O.C., "A Note on the Numerical Computation of Elastic Contact Problems ", Int. J. Num. Meth. Engg., Vol-9, Page 913-924, 1975

15. Okamoto N. and Nakazawa M., "Finite Element Incremental Contact Analysis with Various Frictional Conditions ", Int. J. Num. Meth. Engg., Vol-14, Page 337-357, 1979.

16. Hung N.D. and Sauxe G., "Frictionless Contact of Elastic Bodies by Finite Element Method and Mathematical Programming Techniques ", Computers and Structures, Vol-11, Page 55-67, 198Ø.

17. Sachdeva T.D., Ramakrishnan C.V. and Natrajan R., "A Finite Element Method for the Elastic Contact Problems ", J. of Appl. Mech., Vol-1Ø3, Page 456-461, 1981.

18. Sachdeva T.D. and Ramakrishnan C.V., "A Finite Element Solution for the Two Dimensional Elastic Contact Problems with Friction ", Int. J. Num. Meth. Engg., Vol-17, Page 1257-1271, 1981.

19. Torstenfelt B., "Contact Problems with Friction in General Purpose Finite Element Computer Program ", Computers and Struct., Vol-16, Page 487, 1983

2Ø. Rahman M. V., Rowlands R.E. and Cook R.D., "An Iterative Procedure for Finite Element Stress Analysis of Frictional Contact Problems ", Computers and Struct., Vol-14, Page 947-954, 1984.

21. Chandrasekhara N., Haister W.E. and Goforth R.E., "A Finite Element Solution Method for Contact Problems with Friction ", Int. J. Num. Meth. Engg., Vol-24, Page 477-495, 1987.

22. Vyas N.S., "Vibratory Stress Analysis and Fatigue Life Estimation of Turbine Blade " , Ph. D. thesis, Dept. of Mech. Engg. , I.I.T. Delhi, 1986.

23. Carnegie W., "Vibration of Rotating Cantilever Blading : Theoretical Approaches to the Frequency Problem Based on Energy Methods ", J. Mech. Engg. Sci., Vol.-1, No. 3, 1959.

24. Timoshenko S., Young D.H. and Weaver W., "Vibration Problems in Engineering ",4th Edition, John Wiley, New-York, 1974.

25. Ramesh M.D., "Finite Element Analysis of A Machine Tool Joint as a Contact Problem ", M.Tech. thesis, Dept.of Mech. Engg., I.I.T. Kanpur, 1988.